A NEW METHOD FOR HYDROXYCHLOROQUINE DETECTION

A THESIS SUBMITTED TO
THE GRADUATE SCHOOL OF NATURAL AND APPLIED SCIENCES
OF
MIDDLE EAST TECHNICAL UNIVERSITY

BY

DİLEK ÜNAL TAŞ

IN PARTIAL FULFILLMENT OF THE REQUIREMENTS
FOR
THE DEGREE OF MASTER OF SCIENCE
IN
CHEMISTRY

FEBRUARY 2022

Approval of the thesis:

A NEW METHOD FOR HYDROXYCHLOROQUINE DETECTION

submitted by **DİLEK ÜNAL TAŞ** in partial fulfillment of the requirements for the degree of Master of Science i**n** Chemistry**, Middle East Technical University** by,

Prof. Dr. Halil Kalıpçılar
Dean, Graduate School of **Natural and Applied Sciences** ________________

Prof. Dr. Özdemir Doğan
Head of the Department, **Chemistry** ________________

Assoc. Prof. Dr. Özgül Persil Çetinkol
Supervisor, **Chemistry, METU** ________________

Examining Committee Members:
Prof. Dr. Ayşen Yılmaz
Chemistry, METU ________________

Assoc. Prof. Dr. Özgül Persil Çetinkol
Chemistry, METU ________________

Prof. Dr. İrem Erel Göktepe
Chemistry, METU ________________

Assoc. Prof. Dr. Salih Özçubukçu
Chemistry, METU ________________

Assist. Prof. Dr. Bilge Baytekin
Chemistry, Bilkent University ________________

Date: 09.02.2022

I hereby declare that all information in this document has been obtained and presented in accordance with academic rules and ethical conduct. I also declare that, as required by these rules and conduct, I have fully cited and referenced all material and results that are not original to this work.

Name Last name: Dilek Ünal Taş

Signature:

ABSTRACT

A NEW METHOD FOR HYDROXYCHLOROQUINE DETECTION

Ünal Taş, Dilek
Master of Science, Chemistry
Supervisor: Assoc. Prof. Dr. Özgül Persil Çetinkol

February 2022, 73 pages

Silver nanoparticles (AgNPs) possess unique physicochemical and optical properties. Their localized surface plasmon resonance (LSPR) signal depends on size, shape and composition of the nanoparticles and may change with the intermolecular interactions providing opportunity to design distinct detection platforms for ions, metabolites or drugs. Here, a facile, cost-effective, rapid colorimetric method based on the citrate capped AgNPs (Cit-AgNPs) was developed for hydroxychloroquine (HCQ) detection in aqueous samples. HCQ is an antimalarial drug that has been used for the treatment of diseases such as malaria, rheumatoid arthritis and lupus. It was also extensively used during the initial phase of COVID-19 pandemic. As any other pharmaceutical, high manufacturing levels of HCQ and its uncontrolled use pose possible environmental problems and could become a public health concern due to its accumulation in water systems in the long run. Consequently, the development of fast, straightforward and sensitive sensors for HCQ in aqueous solutions is still in need. The developed platform within the context of this thesis was selective to HCQ among other drugs and quinoline derivatives under the optimized conditions (30.0 mM NaCl, room temperature, 5 minutes of incubation). Limit of detection (LOD) and linear dynamic range (LDR) of the developed platform were found as 9.2 nM and 18.0-240.0 nM, respectively. The applicability of the sensor was tested on HCQ spiked human urine samples (containing 50.0, 120.0 and 240.0 nM HCQ) since HCQ was mainly eliminated through renal clearance. The recovery range, determined to be as 86-98%, supporting the use of the developed platform for HCQ detection as a simple, rapid, and reliable tool.

Keywords: Hydroxychloroquine, Silver Nanoparticles, Colorimetric Detection, Sensors.

ÖZ

HİDROKSİKLOROKİNİN BELİRLENMESİ İÇİN YENİ BİR YÖNTEM

Ünal Taş, Dilek
Yüksek Lisans, Kimya
Tez Yöneticisi: Doç. Dr. Özgül Persil Çetinkol

Şubat 2022, 73 sayfa

Gümüş nanoparçacıklar (AgNPler) eşsiz optik ve fizikokimyasal özelliklere sahiptirler. Nanoparçacığın boyutuna, şekline ve içeriğine bağlı olan lokalize yüzey plazmon rezonans sinyali nanoparçacığın diğer türlerle etkileşimi sonucu değişiklik gösterebilir. Bu da nanoparçacıkların iyon, metabolit ve ilaç tayini gibi farklı amaçlar için çeşitli şekillerde hazırlanıp kullanılmasına olanak tanır. Bu tez kapsamında, sulu ortamda hidroksilorokininin (HCQ) tespiti için kolay, düşük maliyetli, hızlı bir yöntem geliştirilmiştir. HCQ sıtma, romatoid artrit ve lupus tedavisinde kullanılan bir ilaçtır. Ayrıca COVID-19 pandemisinin başlangıcında, tedavi amaçlı olarak tüm dünyada yoğun bir şekilde kullanılmıştır. Diğer ilaçlarda olduğu gibi, yüksek üretim seviyeleri, kontrolsüz kullanımı, ve uzun vadede su sistemlerinde birikmesi nedeniyle çevre sorunlarına neden olması ve de bir halk sağlığı sorunu haline gelmesi olasıdır. Bu sebeple de HCQ'nun özellikle sulu çözeltilerdeki tespiti için hızlı, basit ve hassas sensörlerin geliştirilmesine ihtiyaç duyulmaktadır. Bu tez kapsamında geliştirilen platformun optimize edilmiş koşullar altında (30.0 mM NaCl, oda sıcaklığı, 5 dakika inkübasyon) belirli ilaçlar ve kinolin türevleri arasından HCQ'ya karşı seçici olduğu belirlenmiştir. Geliştirilen sensörün LOD ve LDR değerleri sırasıyla 9.2 nM ve 18.0-240.0 nM olarak hesaplanmış ve uygulanabilirliği, HCQ'nın büyük bir miktarının vücuttan renal klirens yolu ile atılmasından dolayı, HCQ eklenmiş insan idrar numuneleri (50.0, 120.0 ve 240.0 nM HCQ) üzerinde test edilmiştir. Geri kazanım değerlerinin %86-98 aralığında olması geliştirilen platformun HCQ tespiti için basit, hızlı ve güvenilir bir araç olarak kullanılabileceğini göstermiştir.

Anahtar Kelimeler: Hidroksiklorokin, Gümüş Nanoparçacıklar, Kolorimetrik Tespit, Sensörler.

To my past, present and future…

ACKNOWLEDGMENTS

I would like to pay my special regards to Assoc. Prof. Dr. Özgül Persil Çetinkol for her valuable guidance, kindness, patience, encouragement and mentoring throughout the study.

I am grateful to Dr. Mehrdad Forough for his sharing, guidance, friendship, encouragement and support.

My special thanks are extended to all OPC Research Group members, especially to Kübra Doğan, Zeynep Suvacı, Zeynep İrem Bulut, Selin Küçükerenköy and Saba Orouji for their friendship, help and support.

I would like to thank Prof. Dr. İrem Erel Göktepe for her support and valuable reviews, and to her and to members of Erel Research Group, especially Çağrı Turan and Gökçe Tidim, for providing an opportunity for DLS and Zeta potential experiments.

I would like to present my special thanks to Seçkin Öztürk for his friendship and efforts during TEM analysis.

I also wish to thank to Ramazan Altuntaş and World Medicine (İstanbul) for providing the drugs.

I would like to thank METU Health Center for providing the urine samples for application of our method.

I am thankful to the Department of Chemistry, METU for facilities and all the staff for their cooperation and support.

I would like to thank to the thesis evaluation committee members for their contributions.

Finally, I would like to thank to Tayfun Taş for his limitless trust in my abilities and for his support, especially in the final stage of this study.

TABLE OF CONTENTS

LIST OF TABLES

TABLES

LIST OF FIGURES

LIST OF ABBREVIATIONS

8HQ: 8-Hydroxyquinoline

AgNPs: Silver nanoparticles

API: Active Pharmaceutical Ingredient

ASA: Acetyl salicylic acid

AuNPs: Gold nanoparticles

BQ: Biquinoline

Cit-AgNPs: Citrate capped silver nanoparticles

COVID-19: Coronavirus disease 2019

DLS: Dynamic light scattering

EtOH: Ethanol

FAV: Favipiravir

FDA: U.S. Food and Drug Administration

GC: Gas chromatography

HCQ: Hydroxychloroquine

HPLC: High performance liquid chromatography

IVM: Ivermectin

LDR: Linear dynamic range

LOD: Limit of detection

LPV: Lopinavir

LSPR: Localized surface plasmon resonance

PBS: Phosphate-buffered saline

RTV: Ritonavir

SPR: Surface plasmon resonance

Q: Quinoline

UV-Vis: Ultraviolet and visible region

CHAPTER 1

INTRODUCTION

1.1 A Brief Introduction to Nanotechnology and Nanomaterials

The word nano means dwarf in Greek and it refers to the one billionth of a unit as a prefix [1]. Today it is commonly used for describing materials having at least one dimension in the range of 1-100 nm (nanomaterials) and the fields dealing with studies and applications of those materials (nanoscience, nanotechnology, nanomedicine, etc.). The concept, nanotechnology, was first introduced by Richard Feynman in a lecture with the title "Plenty of Room at the Bottom" at the annual meeting of American Physical Society in 1959 [2]. It was not until 1974 that nanotechnology was used as a term and defined by Norio Taniguchi with the following words: "Nanotechnology mainly consists of the processing of separation, consolidation, and deformation of materials by one atom or one molecule" [3]. Although they turned into terms later, nanotechnology and nanomaterials had already been discovered centuries ago. Ancient civilizations used nanostructures to colorize glass and ceramics, and to enhance mechanical strength of their weapons [4-6]. After Feynman's challenging proposal, a growing interest on the small structures, their properties and potential applications emerged. The research rate accelerated with the invention of microscopic characterization methods [7]. In the present day, nanomaterials build up one of the most popular research topics in science and technology.

1.1.1 Nanomaterials

Nanomaterials are structures with at least one dimension within the range of 1-100 nm [8]. They can be in various forms such as nanoparticles (spheres, prisms, cubes, etc.), nanofibers, nanosheets (graphene) or nanotubes (carbon nanotubes), showing different optical, mechanical and electrical properties from their bulk. Nanomaterials can be produced by two approaches: bottom up and top down [9, 10]. In bottom up approach, complex structures are prepared from atoms and molecules through various methods such as wet synthesis, electrodeposition, vapor deposition, etc. Top down approach includes peeling or cutting the bulk material into nano-sized structures as in the preparation of graphene from graphite by adhesive tapes [11]. High energy releasing processes (fires, explosions, welding, etc.), erosion, milling and grinding also produce nanoparticles [12, 13].

Various materials can be used in the production of nanostructured materials. Metals, metal oxides, carbon, polymers, lipids and proteins frequently appear in nanostructures [8]. Availability of diverse materials enables the design and engineering of nanomaterials with different properties for several fields, including medicine, pharmaceutics, electronics, building supplies and textile fibers [14-21]. Compositions of nanomaterials might be varied with the site and purpose of application. For example, metal nanoparticles can be coated with polymers or organic molecules to enhance biocompatibility for in vivo applications such as imaging or drug delivery [14-17], graphene sheets can be doped with ions to increase conductivity in electronic applications [18, 19], or silica nanoparticles can be added to concrete to enhance the mechanical strength while carbon nanotubes have been useful for crack prevention [20]. Dendrimers, the polymeric nanoparticles, are excellent media for drug delivery and imaging due to their solubility and stability in biological environments, low cytotoxicity and polyvalency involved in electrostatic interactions with target structures [22]. Lipid-based nanoparticles and exosomes are commonly employed as drug and nucleic acid carriers with high biocompatibility [23-26]. Nanomaterials involving biodegradable polymers are preferred for applications including tissue scaffolds and wound dressings that will provide support until efficient healing. For example, Xu et al. prepared a vessel scaffold with poly(l-lactid-co-ε-caprolactone) copolymer fibers. Fibers mimicking the size and the orientation of the vessel were found to be favorable for the growth of human coronary artery muscle cells [27]. Hydroxyapatite nanoparticle-polymer composites can be used for bone growth where hydroxyapatite content, which is also a natural component of bone, behaves as a seed [28]. Materials used for wound dressings may include AgNPs for their antimicrobial properties and a combination of biodegradable polymers and other reagents to promote tissue healing and provide mechanical strength and elasticity to the dressing [29]. In brief, the variability of synthesis methods and starting materials, their large surface areas, the possibility of functionalizing their surface, their availability in various shapes and sizes have led to the use of nanomaterials applicable in many different areas, from drugs [16] and house paints [30] to self-cleaning textiles [31].

Among different nanomaterials, nanoparticles especially the AgNPs that are used as the sensing platform in our studies will be discussed in more detail in the following sections.

1.1.2 Nanoparticles

Nanoparticles are particles that have size between 1 and 100 nanometres in diameter [20]. They have attracted great interest during the past few decades due to the wide range of available materials, versatility, facile preparation and variability of modifications according to the field of use. There are various examples of applications in several fields including electronics, medicine and engineering. Nanometer scale size and increased surface area to volume ratio affects the interactions between nanoparticles and the medium. The large surface area promotes reactivity and the catalytic properties [32, 33].

Nanoparticles differ in size, shape and composition resulting in distinct chemical and physical properties. They can be prepared by inorganic or organic materials or a combination of both, and in different shapes (spheres, cubes, stars, etc.) [8, 34].

Among all nanoparticles, spheres are the easiest to synthesize since they have only one dimension that needs to be adjusted by varying the type, the amount of reagents (primary material, coating agent, stabilizing agent, solvent, etc.) used and temperature. To synthesize stars, cubes, etc. both the size and the aspect ratio should be tuned into the desired values, making the reaction condition adjustment more challenging than that of the spheres. Shape of the nanoparticles plays an important role in nanoparticles' orientation in a solution [35], modification capability and in its interactions with the environment while chemical composition determines the surface charge, the extent of the surface interactions and aggregation behavior [8]. The type of material is selected to produce the most suitable particle with the appropriate charge, reactivity, and compatibility for the intended use. For instance, metallic nanoparticles are suitable for catalysis due to their excellent coordination capabilities, while drug delivery efficiency can be improved by tailoring the coating of a nanoparticle for accurate targeting [36, 37].

In our study, AgNPs were used for developing a sensing platform for HCQ detection. Before moving to the following sections, metallic nanoparticles and their distinct properties are worth to be mentioned.

1.1.3 Metallic Nanoparticles

Metals differ from the other common materials used for nanoparticle synthesis with their magnetic and optical properties [36, 38]. Their ligand binding properties are advanced due to unoccupied orbitals of the metal atoms, which will allow them to act as Lewis acids. The interaction between the ligand and the metal atom can result in the quenching of optical activity of the metal, enhancement of that of the ligand or vice versa [40, 41]. Those changes make a useful tool for monitoring the metal-ligand interactions, ligand exchange processes, and stability and reactivity of the nanoparticles. Metallic nanoparticles have various applications in catalysis, imaging, therapeutics and wastewater management [32, 37, 38, 40]. Their toxicity depends on the size, composition and the exposure dose of the particle [42].

The use of metallic nanoparticles in sensing applications commonly takes advantage of their distinct optical properties and strong localized surface plasmon resonance (LSPR). LSPR signals arise as a result of the interaction of light with the electrons of small (with a diameter lesser than the wavelength of incident light) metallic particles. Oscillating electric field of the incident light induces a coherent oscillation of conduction electrons of the particle [43]. LSPR signals of metallic nanoparticles can be altered with exogenous factors. The altered LSPR signals generally provide information about the nanoparticles' size and aggregation and allow the use of those nanoparticles as sensors and detection platforms for various substances [44, 45].

Among the metallic nanoparticles, gold and silver nanoparticles (AuNPs and AgNPs) are two of the most commonly exploited. They are preferred in sensing applications due their optical and physiochemical properties that can be tuned by changing the size, shape and composition [44-47]. AuNPs have significant affinity for thiol (-SH) and amine (-NH_2) groups while AgNPs can attract a variety of groups including carboxylates (-COO^-), hydroxyls (-OH), amines (-NH_2) and thiols (-SH) [47-54]. Most of AuNPs synthesis procedures require heating or boiling around 80-100 °C. On the other hand, one of the common synthesis methods for AgNPs is $NaBH_4$ reduction in the presence of a stabilizing agent in an ice bath at around 0 °C. Both particle systems are sensitive to light and should be stored in dark to avoid light dependent decomposition. Compared to AuNPs, AgNPs are cost-effective, easier to prepare and more stable at various conditions for a prolonged period of time [49, 54, 55].

1.2 Silver Nanoparticles as Sensors

AgNPs have been frequently employed for numerous purposes including analytical, biomedical, therapeutic applications with no or slight modifications to enhance stability, sensing ability or optical properties [57-66]. Their varying color mainly with the size and shape makes them excellent candidates for sensors and detection systems [44, 45, 60]. It allows monitoring the interactions between AgNPs and analyte, in some cases even with naked eye, making the AgNPs suitable platforms especially for quick in-situ detections. In recent decades, AgNPs have gained huge interest in the development of optical detection platforms for pharmaceutical compounds and various analytes (mainly environmental pollutants and biomolecules) due to their tunable optical properties attributable to their unique LSPR peaks. In general, spherical AgNPs in the size range of 10-20 nm have been reported to exhibit an LSPR absorption band with a maximum of 390-400 nm [67]. The position of the absorption peak of AgNPs depends on their size and shape as well as the local dielectric environment [68]. Another key factor in the application of AgNPs in optical sensing applications/platforms is the use of an organic ligand/modifier as a stabilizing agent during their preparation steps.

One of the recent applications AgNPs as a sensitive sensing platform was based on the use of folic acid-modified AgNPs for the colorimetric determination of 6-mercaptopurine (a sulfur analog of adenine used as an anticancer agent and immunosuppressant) in the range of 20-1000 nM in urine samples with an LOD of 13.2 nM. The mechanism of action of this probe is based on the oxidation of the Ag^0-Ag^+ ions, resulting in a distinct blue shift of the SPR peak and an observable color change from yellow to colorless [69].

In another study, Pb^{2+} and Hg^{2+} ions were detected in aqueous samples with AgNPs prepared with the root extract of *Bistorta amplexicaulis* plant which was used as the reducing and capping agent. The SPR signal of AgNPs decreased and the color of the solution changed from brown to yellow due to the interactions of Pb^{2+} with AgNPs. However, Hg^{2+} ions are observed to oxidize Ag^0 to Ag^+ ions and deposited on the surface of the nanoparticle. Color of the solution faded as the degree of Ag^0 oxidation increased. In this case, a decrease, a shift and broadening in the SPR signal were observed [61]. Another study reported a sensor based on the reverse binding mechanism. The ligand, dithizone, was coordinated to Pb^{2+} ion and aggregation was observed after the addition of AgNPs. The interaction of AgNPs with sulfur atoms of dithizone molecules result in a significant decrease in the SPR band and formation of a weak broad band at longer wavelengths. The limit of detection and the limit of quantification were reported as 0.64 ± 0.04 μg/L, and 2.1 ± 0.15 μg/L, respectively

[62]. AgNPs were also used as sensing platforms in pesticide detection in water and soil. Kodir et al. [63] showed that the positively charged moieties of cypermethrin interact with negatively charged groups of the capping agent, L-cysteine, to disturb the nanoparticle stability and induce aggregation within the cypermethrin concentration range of 0 - 100 ppm [63].

Biomolecules such as DNA, metabolites or amino acids can also be detected with AgNPs. Li et al. [53] reported the detection of tryptophan by 4,4-bipyridine-functionalized AgNPs with a colorimetric limited detection concentration of 2×10^{-5} M. The color of modified AgNPs solution turned to red from yellow with the addition of tryptophan. The SPR signal around 394 nm decreased and a broad band centered at 556 nm appeared [53]. Eswaran et al. proposed a method for L-histidine detection using sebacic acid-capped AgNPs. In their study, AgNPs had an affinity for both sebacic acid and L-histidine, whose amine and carboxylic acid groups also interacted with each other via hydrogen bonding interactions. The interactions led the aggregation of AgNPs reducing the SPR signal with the increasing concentration of L-histidine. The interactions resulted in the aggregation of AgNPs, causing the SPR signal to decrease with increasing concentration of L-histidine. The lowest detection limit was reported to be as 122 nM [64].

1.3 Silver Nanoparticles in Drug Detection

Drug sensor development is an active area of research in both academic and industrial laboratories. The design of detection platforms for critical care drug monitoring, clinical evaluation, process control, quality assurance, and environmental toxicity detection has advanced in recent years. Sensors for the detection of Active Pharmaceutical Ingredients (APIs) have also become important due to the increasing manufacturing, uncontrolled use, and their release to the environment [67, 68]. An Active Pharmaceutical Ingredient (API) is defined as “any substance or mixture of substances intended to be used in the manufacture of a drug product and that, when used in the production of a drug, becomes an active ingredient in the drug product. Such substances are intended to furnish pharmacological activity or other direct effect in the diagnosis, cure, mitigation, treatment or prevention of disease or to affect the structure and function of the body" by FDA [70].

Several sensors have been developed so far for the quantification of APIs in the finished drug product. Examples include sensors for the detection of aspartate, glucose, salicylic acid, and acetylsalicylic acid, ephedrine, and antibiotics [71, 72]. Sensors have also been developed for the detection of APIs in urine and water samples [54, 69]. Urine analysis is a nonivansive and powerful clinical diagnostic tool. It is well suited for point-of-care (PoC) monitoring applications especially in the diagnosis of various urologic and renal conditions since the excretion of drugs through kidneys is the primary route of elimination from the body for many drugs [73].

A comprehensive review of the literature shows that the use of AgNPs (with applicability in various matrices) has also been the focus of the development of such optical nanosensor platforms over the last two decades [60-66]. Sharp and intense LSPR signal of small AgNPs has been a perfect tool for detection of various pharmaceutical compounds/active ingredients. As mentioned in the previous sections, the LSPR signal is strong and sensitive to environmental changes. The alterations in the existing LSPR signal of the nanoparticle are found to provide information about the AgNPs-API/drug interactions. There are several studies employing the AgNPs' LSPR change in drug detection. For example, Moraes et al. used glutathione (GSH)-stabilized AgNPs to determine three antibacterial drugs, fluoroquinolones; ciprofloxacin (CIP), norfloxacin (NOR) and enrofloxacin (ENRO), simultaneously. SPR band at 400 nm exhibited a red shift upon the addition of the drug molecules. Fluoroquinolones replaced GSH molecules on the surface of the AgNPs which resulted in the aggregation of AgNPs through Van der Waals interactions. LODs were calculated as 0.397, 0.437 and 0.398 μmol/L and LOQs were 1.203, 1.323 and 1.205 μmol/L for CIP, NOR and ENRO, respectively [74]. Ganizadeh et al. [52] detected zidovudine (ZDV), an antiviral drug against HIV, with AgNP-modified β-cyclodextrin (β-CD). LSPR signal of AgNP at around 405 nm decreased and another band with the maximum absorption at 560 nm appeared in the presence of ZDV. The color of the solution turned from yellow to red. The changes in the UV-Vis spectrum and the color were explained by the impaired interactions between AgNPs and the hydroxyl groups of β-CD upon the addition of ZDV. In the absence of ZDV, AgNPs were coordinated by -OH groups of β-CD. The addition of ZDV, results in the coordination of the β-CD molecular cavities, loosening AgNP-OH interactions and causing aggregation. The LDR was reported to be 50-500 μM and LOD as 42 μM [52]. Shrivas et al. [54] used AgNPs to detect ampicillin in urine samples. They showed that LSPR band of Cit-AgNPs shifted to a longer wavelength and the color of solution turned from yellow to pink after the addition of ampicillin spiked into urine samples due to the aggregation of AgNPs. In their study, the aggregation process was reported to be due to the hydrolysis of ampicillin to penicillamine at pH 4. The sulfur moiety of penicillamine is reported to disturb and replace the citrate capping of Cit-AgNPs, triggering the aggregation. The method had a linear range of 25-1200 ng/L and a LOD of 10 ng/L [54].

As shown in the studies reported above, AgNPs are commonly exploited as an alternative in the development of sensitive drug detection platforms. The reported platforms mostly depend on the ligand binding or ligand loss that might be accompanied by aggregation. AgNPs were shown to interact with different ligand moieties including amine and hydroxyl groups which are also present in the molecular structure of previously mentioned drugs [52, 54, 74]. In general, the presence of the ligand is reported to decrease the colloidal stability of AgNPs and alter (decrease, broadening or a red shift) the LSPR signal. The formation of new absorption bands at longer wavelengths can also be observed as a sign of interactions between the ligand and AgNPs. And, such changes in the LSPR signal provide simple, straightforward detection platforms [54]. Accordingly, based on the aforementioned studies, AgNPs are thought to be a promising candidate platform for HCQ detection.

1.4 Hydroxychloroquine

Hydroxychloroquine (HCQ) (Figure 1), a drug which belongs to the family of antimalarials, has been widely used for the treatment of diseases such as malaria, porphyria, rheumatoid arthritis and lupus [75]. It was also highly popular in the last two years due to its initial use in COVID-19 treatment until FDA revokes emergency use authorization for HCQ after the identification of heart rhythm problems as a frequent side effect. In addition to its anti-inflammatory and immune response reducing effects, HCQ has been shown to possess antiviral activity against various viruses, such as human immunodeficiency virus (HIV), hepatitis A virus, hepatitis C virus, influenza A and B viruses, influenza A H5N1 virus and various others [76]. It is a weak base which is known to influence the acidic vesicles and lysosomal activity and has role in the inhibition of many enzymes such as glycosyl-transferases and proteases [77, 78].

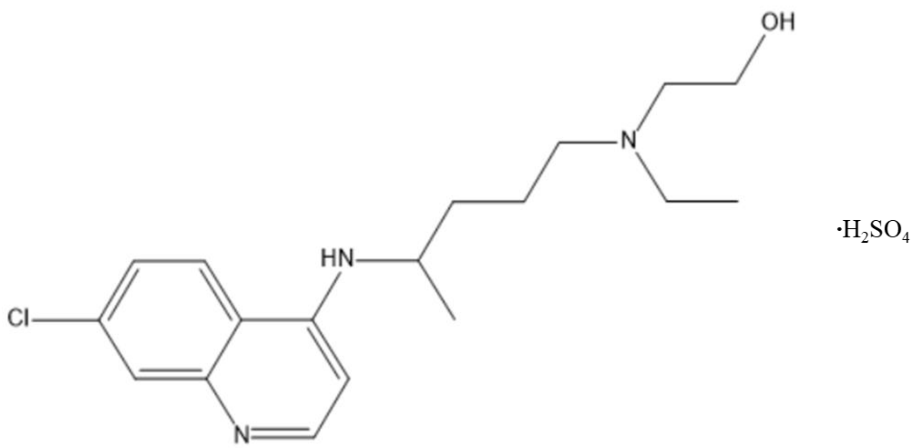

Figure 1: Chemical structure of hydroxychloroquine sulfate.

HCQ is a derivative of quinine which was obtained from the cinchona tree. It was introduced to the European world after the bark powder had been used for the treatment of a malarial colonial in 1638. Quinine was first isolated by French scientists Pierre Joseph Pelletier and Joseph Bienaimé Caventou in 1820 and remained the major drug for malaria treatment for over a century. Chemical synthesis of methylene blue, a dye and a therapeutic, by Heinrich Caro in 1876 brought out the idea of synthetic quinine which resulted in the synthesis of several drugs with similar molecular structures, such as chloroquine, during 1930s. After the toxicity of chloroquine was revealed, the search for a less toxic option was started. In 1945, hydroxylation of chloroquine yielded HCQ. In 1950s, HCQ had its part in the treatment of lupus first, and then another familiar disease, rheumatoid arthritis. However, long use of HCQ and high doses were proven to cause retinal damage. During 1980s, the dosage adjustment and the usage of combination of drugs instead of only HCQ were accepted as a less harmful and more reliable treatment method [79-83]. HCQ have been commercially available under several brand names and it was one of the most commonly prescribed antiviral drugs at the beginning of the COVID-19 pandemic period. Especially, health workers were encouraged to use HCQ for prevention [84].

HCQ is prescribed to rheumatoid arthritis and systemic lupus patients as hydroxychloroquine sulfate in the form of a 200 mg oral tablet and the number of 200 mg tablets consumed in a year was as high as 500 million even before the pandemic. The drug reaches its peak levels in the blood in healthy males 3.26 hours after administration and it has a blood half-life of 22 days. Only 25–45% of HCQ undergoes long term storage in fat free tissues. Like other 4-aminoquinolines, HCQ is metabolized and excreted through the liver and the kidneys. 40–60% of the drug is excreted in raw form or in the form of metabolites in the urine; 8–25% in raw or metabolized forms in the feces and 5% is lost through the skin. If kidneys or liver do not function properly, level of HCQ retention in the body increases as well as the risk of side effects including retinopathy and cardiovascular problems arising as a result of overdose as mentioned above [85-87]. Therefore, we hypothesize that since

HCQ was mainly excreted in the urine, developing a simple method for detection of HCQ can be an important tool in diagnostic applications [87, 88].

Studies revealed that those who had consumed HCQ experienced nausea, diarrhea, abdominal pain, alterations in blood glucose levels and palpitations in short term use (days to weeks) while long term use (years) was shown to cause retinopathy, cardiomyopathy and some minor neurological indications. If HCQ is consumed in higher doses than recommended, it is reported to possibly cause cardiovascular shock and collapses which might be fatal [86, 87].

Even though HCQ has good bioavailability, it reported to be significantly toxic in patients with plasma levels ranging between 2.05 and 18.16 μmol/L (640 μg to 6100 μg/L) and fatalities with postmortem blood levels of 142.89 μmol/L (48,000 μg/L) and 309.62 μmol/L (104,000 μg/L) [89]. The risk of toxicity from the regular use of HCQ in malaria and lupus is reported to be low. However, its use, especially its widespread non-prescription use during the initial phase of the pandemic at very high doses raised concerns regarding its toxicity [87, 89-91]. On the other hand, HCQ was manufactured at about 300 tonnes mainly in India per year for use in the treatment of malaria and lupus [92, 93]. However, its interim use in COVID-19 pandemic resulted in a sudden increase in its global production. Several API producers reported to ramp up their production. For instance, Zydus Cadila reported to increase its production from 3 metric tonnes per month to 20 to 30 metric tons per month [94, 95].

In general, the uncontrolled use, manufacturing and release of pharmaceuticals have become public health concern due to their accumulation in water systems and human food chain [96]. Their effects on the health of ecosystems and humans are presented as deleterious [97-99]. The emergence of microbial resistance due to antibiotics or the effect of hormonal contraceptives on the endocrine system as the observed feminization of fish in rivers can be given as two of the obvious examples [98]. Just recently, Wilkinson et.al. [99] reported in PNAS that pharmaceutical pollution poses a global threat to environmental and human health by sampling 1052 sites along 258 rivers in 104 countries of all continents, representing the pharmaceutical fingerprint of 471.4 million people. They found out that the concentrations of at least one API at 25.7% of the sampling sites were greater than concentrations considered safe for aquatic organisms, or which are of concern in terms of selection for antimicrobial resistance [99]. They also revealed the importance of the use of a minimized-design sampling protocol with rapid and cost-effective analytical methodologies in such studies.

High manufacturing levels of HCQ might well also cause environmental problems in the long run. Moreover, the high levels of HCQ in the environment might cause antimalarial drug resistance that has emerged as one of the main challenges in malaria control [100-102]. Accordingly, due to the wide-ranging clinical potential of HCQ and the environmental risks mentioned, the development of simple and novel analytical detection methods will be valuable to detect HCQ concentrations in biological fluids, environmental samples and dosage forms. Consequently, detecting HCQ using a non-invasive methods and simple spectrophotometric methods might also be advantageous. To date, several analytical methods have been reported for monitoring and detecting HCQ in biological matrices and pharmaceutical formulations. These techniques include chromatographic, electrophoretic, electroanalytical, spectrometric, and enzyme-linked immunosorbent assay (ELISA) tests, and are discussed in more detail in the next section.

1.4.1 Methods for Hydroxychloroquine Detection

Methods used for HCQ detection include mainly chromatographic and electrochemical methods. Several chromatography-based approaches including high performance liquid chromatography (HPLC) with various detection modes (UV, DAD and FL), capillary electrophoresis (CE), liquid chromatography-tandem mass spectrometry (LC-MS), ultra-performance liquid chromatography (UPLC) and other hyphenated techniques have been reported for the quantification of HCQ in various matrices (plasma, serum, urine, whole blood and tissues of human and rat) as well as pharmaceutical dosage forms [103-107]. The evaluation of the presence of HCQ in biological media is of great importance and selecting the most suitable analytical method for determining this drug with high accuracy is crucial.

In chromatography-based approaches, a separation process is carried out with the cshromatographic section of the instrumentation first and then the detection is performed with MS, UV or FL [108-110]. For reliable detections, sample preparation, microextraction, matrix elimination and separation processes require certain time and labor. Specific solvents, generally toxic ones, are used in large amounts for purification and separation steps, bearing environmental concerns. For instance, the LOD for HCQ were found as 10 ng/mL and 1 ng/mL in different studies conducted by Williams et al. and Tett et al., respectively, both employing HPLC and FL with same type of column but with different extraction techniques and different mobile phases [105,106]. Williams et al. used hexane: methyl tert-butyl ether (1:1) for extraction and methanol-water (80:20), with 100 mM triethylamine, adjusted to pH 11 with 1 M sodium hydroxide as mobile phase while Tett et al. used diethyl ether and 0.5% n-butylamine in methanol-hexane-methyl tert-butyl ether (1:l:l). Multiple extraction steps were required for higher recovery of HCQ from the original samples. Selectivity can be a problem in chromatographic methods when similar molecular structures exist in the matrix. Chiral columns and modified mobile phase systems can be used to enhance selectivity, which are especially useful for the separation of different isomers of a drug produced during the synthetic processes [107]. However, they are expensive or should be tailor-made for the analyte.

Electrochemical techniques also have been frequently used for the detection and determination of chloroquine-based drugs especially HCQ. Arguelho et al. presented electrochemical reduction of HCQ using a glassy carbon electrode (GCE) and reported a linear concentration range from 2×10^{-5} to 5×10^{-4} M, with a LOD of 11.2 μg/mL [111]. Mashhadizadeh et al. investigated an electroanalytical methodology for the determination of chloroquine using differential pulse voltammetry (DPV) at $Cu(OH)_2$ nanowire-modified carbon paste electrode. Based on their results, chloroquine showed a linear range from 0.068 to 6.88 μg/mL with a LOD of 0.01 μg/mL [112]. Deroco et al. have reported a square wave voltammetry (SWV) method for the determination of HCQ with a cathodically pretreated boron doped diamond electrode. In their study, the obtained SWV analytical curve presented a linear response from 0.1 to 1.9 μM, with a LOD of 0.06 μM [113]. In another study, HCQ determination was performed by using glassy carbon electrode (GCE) using cyclic voltammetry, double potential step chronocoulometry and linear sweep voltammetry (LSV) techniques giving a LOD of 4.65 nM. The prepared modified electrode has been then utilized for detection of chloroquine in human body fluids [114]. A potentiometric determination of hydroxychloroquine sulfate in pharmaceutical preparations and human urine samples was recently reported using a new coated graphite electrode. The linear range was 9.3×10^{-5}-1.0×10^{-2} M with a LOD of 4.7×10^{-5} M [115]. Although they present low LODs, electrochemical detections are performed under strict experimental conditions in terms of electrolyte concentration, temperature, electrode selection, etc. and with relatively expensive instrumentation. Most electrochemical methods require customization of electrodes to improve selectivity, which is a time-consuming, laborious, and high-cost process [116, 117]. Since the availability of the instrumentation and providing the desired experimental conditions are the major issues besides the limitation of applications, electrochemical methods do not appeal to every research group or medical facility especially in the resource-limited environments, such as in developing countries which may lack fully-equipped facilities, trained medical staff and support.

Most of the previously reported methods for HCQ detection are powerful techniques for the analysis of HCQ and CQ. However, they owe their superb performance to the expensive and complex instrumentation and time-consuming, generally multi-step, sample preparation procedures under strict experimental conditions. It is worth noting that the cost-effectiveness, simplicity, and rapidity of the selected techniques play a crucial role in HCQ determination. Today, label-free detection systems with little to no sample preparation and organic solvent consumption are more appreciated. The association of nanotechnology with medical treatment, including therapeutic drug monitoring (TDM), pharmacokinetic and pharmacodynamic studies has provided a new concept in drug detection [54]. Colorimetric methods use the intrinsic advantages of colorful species upon the addition of a certain analyte. In this regard, the use of noble metal nanoparticles (in particular AuNPs and AgNPs) for colorimetric purposes has received great attention [42, 54, 74]. To the best of our knowledge, no studies have reported on the colorimetric and/or noble metal nanoparticles-based UV-Visible spectrometric detection of HCQ and CQ in aqueous, pharmaceutical or biological samples so far. Consequently, we hypothesized that the development of a simple, sensitive and fast colorimetric detection method for monitoring HCQ levels in aqueous solutions might be imperative especially in countries that lack state-of-the-art facilities.

1.5 Scope of the Thesis

HCQ has been a widely used for the treatment of several diseases for almost a century [75]. The production and consumption of HCQ increased considerably since the COVID-19 outbreak and high manufacturing levels might result in environmental problems in the long run [84, 94]. Severeal methods have been developed for HCQ detection so far. However, they necessitate the use of complex instrumentation and generally multi-step, sample preparation procedures [107-115].

The purpose of this study is to develop a facile, rapid, cost-effective and sensitive colorimetric method for HCQ detection in aqueous solutions. To our knowledge, this will be the first report of the development of a colorimetric detection platform using citrate capped AgNPs (Cit-AgNPs). The platform is devised based on the aggregation behavior of the negatively charged citrate capped AgNPs in solution in the presence of HCQ. The aggregation of Cit-AgNPs results in a change in the LSPR intensity that can be easily monitored via UV-Vis spectroscopy accompanied with a color change apparent to the naked eye. The experimental conditions such as NaCl concentration, temperature and incubation time are thought to affect the aggregation behavior of Cit-AgNPs, and therefore are assessed before determining the analytical merits of the platform. Finally, since HCQ is secreted through the urine, we aimed to demonstrate the applicability of the method in human urine samples and its selectivity towards HCQ in the presence of certain drugs and small molecules.

CHAPTER 2

MATERIALS AND METHODS

2.1 Materials

Silver nitrate ($AgNO_3$), sodium borohydride ($NaBH_4$), hydrochloric acid (HCl), biquinoline ($C_{18}H_{12}N_7$) and 8-hydroxyquinoline (C_9H_7NO) were purchased from Merck KGaA (Germany). Tri-sodium citrate dihydrate ($Na_3C_6H_5O_7.2H_2O$), sodium chloride ($NaCl$), sodium hydroxide ($NaOH$), sodium phosphate monobasic (NaH_2PO_4) and sodium phosphate dibasic (Na_2HPO_4) and ethanol (EtOH) were purchased from Sigma Aldrich (USA). Acetyl salicylic acid was purchased from Fischer Scientific (USA) and favipiravir, ivermectin, ritonavir and lopinavir were obtained from Word Medicine (Turkey). Urine samples were obtained from METU Health Center.

Standard stock solutions of all drugs and small molecules were prepared by dissolving required amount of solid in phosphate buffered saline-ethanol solution (PBS:EtOH (70:30, v/v)). Millipore water (Milli-Q, 18.2 MΩ cm^{-1}) was used in all sample preparations including further dilutions unless stated otherwise.

2.2 Methods

2.2.1 Instrumentation

A Cary 8454 UV-Vis photodiode array spectrophotometer equipped with an Agilent 89090A peltier (Santa Clara, CA, USA) was used for acquiring absorption spectra. UV-Vis spectra were collected using a 10 mm quartz cell between 200 and 800 nm. Hermle Z 326 K centrifuge (Hermle Labortechnik, Wehingen, Germany) was used to remove the residues and purify the synthesized Cit-AgNPs solution. A Mettler

Toledo Seven Compact S210 pH meter (Greifensee, Switzerland) was used for pH adjustments and a vortex mixer (Isolab, Germany) was used for the homogenization of mixtures. Cit-AgNPs were characterized by dynamic light scattering (DLS) and zeta potential measurements on Zetasizer Nano-ZS instrument (Malvern Instruments Ltd, Malvern, UK). Thermo Scientific Nicolet IS10 FTIR Spectrometer (Thermo Fischer Scientific, Waltham, Massachusetts, USA) was used for Fourier transform infrared (FTIR) spectra. TEM images were obtained via a Tecnai G^2 Spirit BioTwin CTEM microscope (FEI Company, Oregon, USA) at METU Central laboratory.

2.2.2 Synthesis of Cit-AgNPs

Cit-AgNPs were synthesized through the method previously reported by Flores et al. [51] with minor modifications. Briefly, 25.0 mL of 5.0 mM $AgNO_3$ solution was mixed thoroughly with 400.0 mL of 1.06 mM $Na_3C_6H_5O_7$ solution with continuous stirring in the ice bath at around 0 °C, followed by the dropwise addition of 2500.0 μL of a freshly prepared 100.0 mM aqueous solution of $NaBH_4$ over a 5 min period. The color of the solution changed from colorless to light yellow immediately with $NaBH_4$ addition. The reaction mixture was stirred vigorously in the ice bath in dark for 1 h and 45 min until the color changes to shiny yellow, which indicates the formation of Cit-AgNPs. The solution was then placed in dark at room temperature overnight. Cit-AgNPs solution with a final concentration of 3.16×10^{-2} mg Ag/mL was centrifuged at 8000 rpm for 20 min at room temperature to remove any residues and then diluted in a 1:3 ratio with H_2O. The final AgNP concentration in the nanoparticles suspension before dilution was estimated using a previously reported molar extinction coefficient (ε_{395}) of 10.1×10^{8} M^{-1} cm^{-1} [118]. The synthesized AgNPs were characterized by UV-Vis spectroscopy, high contrast transmission electron microscopy (TEM), Fourier transform infrared spectroscopy (FTIR), dynamic light scattering (DLS) and zeta potential techniques. The synthesized AgNPs were wrapped in aluminium foil and stored at 4 ºC for further use. The stability of AgNPs was checked before use by comparing their UV-Vis spectrum to their UV-Vis spectrum when they were fresly prepared. The stability of the synthesized AgNPs at room temperature and at 4 °C was monitored also in the long term (Appendix A). UV-Vis spectra were collected on a Cary 8454 UV-Vis photodiode array spectrophotometer equipped with an Agilent 89090A peltier (Santa Clara, CA, USA) between 190 and 800 nm. FT-IR spectra were collected using KBr method at a resolution of 4 cm^{-1} between 4000 and 600 cm^{-1} by accumulation of 32 scans. The samples contained ~0.01 mg Ag/mL AgNPs, 30.0 mM NaCl or 200 nM HCQ. The samples used in TEM imaging experiments were also prepared under the same conditions.

2.2.3 Optimization of Experimental Conditions

All experiments (optimization, selectivity, sensitivity and recovery experiments) were performed in triplicate unless otherwise mentioned.

Salt concentration, temperature and incubation time were determined to be the major factors affecting the Cit-AgNPs-HCQ interactions. The synthesized Cit-AgNPs exhibit an absorption maximum at around 395 nm. UV-Vis absorbance and mainly the change in absorbance at 395 nm were monitored to find the optimum conditions [119-121].

To determine the optimum NaCl concentration, different volumes of 1.0 M NaCl solution (0-200.0 μL, 0-66.7 mM final NaCl concentration in 3000.0 μL sample) were added to 2700.0 μL of Cit-AgNPs and the volume was completed to 2900.0 μL with H_2O. The solution was mixed well and then 100.0 μL of 10.0 μM HCQ was added. UV-Vis spectra were recorded for each sample after 10 minutes of incubation time. Control experiments without HCQ were performed under the same conditions.

To determine the effect of time on the developed detection platform, 90.0 μL of 1.0 M NaCl was added to 2810.0 μL of Cit-AgNPs and the mixture was vortexed. Then, 100.0 μL of 10.0 μM HCQ was added to the solution and the absorbance values at 395 nm were recorded at definite time intervals (0.5-60 minutes).

The effect of temperature was determined by monitoring the absorbance of Cit-AgNPs+NaCl+HCQ samples at 395 nm. Briefly, 90.0 µL of 1.0 M NaCl was added to 2810.0 µL of Cit-AgNPs and mixed well with a vortex. Then, 100.0 µL of 10.0 µM HCQ was added to the Cit-AgNPs+NaCl solution. The absorbance at 395 nm was collected at different temperatures (15-75 °C) after 5 minutes of incubation at the given temperature. The absorbance of Cit-AgNPs+NaCl sample at 395 nm was also monitored between 15-75 °C.

2.2.4 Selectivity and Sensitivity

For selectivity experiments, 50.0 µM stock solutions of drugs (HCQ, Acetyl salicylic acid (ASA), Ivermectin (IVM), Favipiravir (FAV), Ritonavir (RTV), Lopinavir (LPV)) and quinoline derivatives (Quinoline (Q), Biquinoline (BQ), 8-Hydroxyquinoline (8HQ)) were prepared first. Then the solutions were diluted to 10.0 µM with H_2O. For each drug and quinoline derivative, 90.0 µL of NaCl was added to 2810.0 µL Cit-AgNPs and mixed thoroughly. Then 60.0 µL of 10.0 µM analyte solution was mixed with 40.0 µL H_2O and added to Cit-AgNPs+NaCl solution. The final drug or quinoline derivative concentration was 200.0 nM. After 5 minutes incubation at room temperature, UV-Vis spectrum was recorded for each sample.

Next, the behaviour of Cit-AgNPs+NaCl+HCQ system was investigated in the presence of other drugs and quinoline derivatives. Solutions containing only drugs, only quinoline derivatives, and drugs and quinoline derivatives together, with and without HCQ were prepared from 50.0 µM stock solutions. 24.0 µL of each species was transferred to the vial and the total volume was completed to 216.0 µL with H_2O. Likewise, the previous steps, 90.0 µL of 1.0 M NaCl was mixed with 2802.0 µL of Cit-AgNPs and 108.0 µL of each solution (drugs, quinolines or drugs+quinolines mixture) was added to Cit-AgNPs+NaCl. The final concentration of each drug or quinoline derivative in 3000.0 µL sample was 200.0 nM. UV-Vis spectrum of each sample was recorded after 5 minutes of preparation.

Cit-AgNPs' sensitivity towards HCQ was investigated by titrating a Cit-AgNP+NaCl solution, which was prepared by mixing 2760.0 µL Cit-AgNPs and 90.0 µL 1.0 M NaCl with 5.0 µL portions of 10.0 µM HCQ (0.0 to 150.0 µL, with final HCQ concentration between 0.0-500.0 nM). UV-Vis spectra were taken after each addition. The absorbance change with HCQ addition with respect to that of Cit-AgNPs+NaCl was calculated from the absorbance values at 395 nm. LDR was determined based on the deviation of data from a straight line. The calibration plot was constructed in the LDR, between 18.0-240.0 nM of HCQ, and simple linear regression was used to estimate the relationship between HCQ concentration and the change in absorbance (ΔA: $A_{(Cit\text{-}AgNPs+NaCl)}$-$A_{(Cit\text{-}AgNPs+NaCl+HCQ)}$) at 395 nm [119-121]. In other words, a linear regression equation was obtained in the LDR range to use in further experiments. LOD was calculated from the concentration at which the absorbance change is 3 times of the standard deviation of the blank [122].

2.2.5 Application of the Method

The method's applicability was tested using human urine samples obtained from three healthy participants at METU Health Center. The original urine samples were extremely concentrated and introduced a complicated and interfering matrix for HCQ detection. First, the urine samples were filtered to remove any organic or insoluble residues and diluted to 1:25, 1:50, 1:100, 1:150 and 1:250 with H_2O to decrease the interference of the matrix [123-126]. For each dilution set, three samples with final HCQ concentrations of 1.5, 3.6 and 7.2 µM were prepared by adding different volumes of HCQ stock solution to 900.0 µL of diluted urine solutions. The total sample volume was completed to 1000.0 µL with H_2O. The solutions for UV-Vis measurement were prepared by mixing 90.0 µL 1.0 mM NaCl and 2810.0 µL Cit-AgNPs and adding 100.0 µL of the diluted urine samples spiked with HCQ. The final HCQ concentrations in the prepared 3000.0 µL samples were 50.0, 120.0, 240.0 nM, respectively. UV-Vis spectra were recorded for each sample before and after the HCQ addition and absorbance values at 395 nm were recorded under the optimized experimental conditions. The calibration curve constructed (previous section) and the linear regression equation obtained was used in calculating HCQ concentrations. Recovery is expressed as the amount of analyte found as a percentage to the theoretical amount thought to be present in the medium. The relative recovery is defined as the measured concentration of the drug(s) divided by their actual concentrations and expressed in percentage. In this study, recovery percentages were calculated for each sample by using the theoretical and experimental HCQ concentrations using the following equation: Recovery (%) = 100 × found value/nominal value. RSD, the relative standart deviation of the mean, for the recovery values were calculated using the following equations:

$$SD = \sqrt{\frac{\sum(x_i - \bar{x})^2}{N-1}} \qquad \text{(Eq. 2-1)}$$

$$RSD\ \% = \frac{SD}{\bar{x}} \times 100 \quad \text{(Eq. 2-2)}$$

Here; $\Sigma =$ sum of

$x_i =$ value of each data set

$\bar{x} =$ mean of the data set

N = number of data points

SD = Standard deviation

RSD % = Percent relative standard deviation

CHAPTER 3

RESULTS AND DISCUSSION

3.1 Colorimetric Detection of Hydroxychloroquine - Overview

Cit-AgNPs with a diameter as small as 10-20 nm exhibit a unique LSPR signal around 390-400 nm. The synthesized Cit-AgNPs had a UV-Vis spectrum which is consistent with the Cit-AgNPs introduced in previous studies (Figure 2) [51, 118, 123]. Cit-AgNPs and the change in their LSPR signal upon the addition of analytes were used to develop sensitive detection platforms previously [52-54, 60-64].

Our initial studies with Cit-AgNPs and HCQ suggested that the change in the LSPR signal of Cit-AgNPs could also be a plausible detection platform for HCQ. Samples were prepared by mixing 90.0 μL 1.0 M NaCl with 2810.0 μL Cit-AgNPs followed by the addition of 100.0 μL 10.0 μM HCQ. The total volume was completed to 3000.0 μL with H_2O in the control samples that did not contain either NaCl or HCQ (Figure 2 and Figure 3). The samples were then incubated for 5 minutes and the UV-Vis spectra and the photograph were taken afterwards.

As demonstrated in Figure 2, AgNPs give rise to a sharp LSPR signal (black line). A slight decrease, indicating the interactions of HCQ with Cit-AgNPs, was observed in the intensity of the LSPR signal upon the addition of HCQ onto Cit-AgNPs (red line). The decrease in intensity accompanied with the broadening of the signal was remarkable upon addition of HCQ in the presence of NaCl (green line). These changes observed in the UV-Vis spectrum of AgNPs+NaCl+HCQ (green spectrum), compared to UV-Vis spectrum of Cit-AgNPs +NaCl (blue spectrum), suggested the aggregation of Cit-AgNPs upon the addition of HCQ in the presence of NaCl [128-132]. The role of NaCl in aggregation behavior of Cit-AgNPs is going to be explained in detail in the following sections.

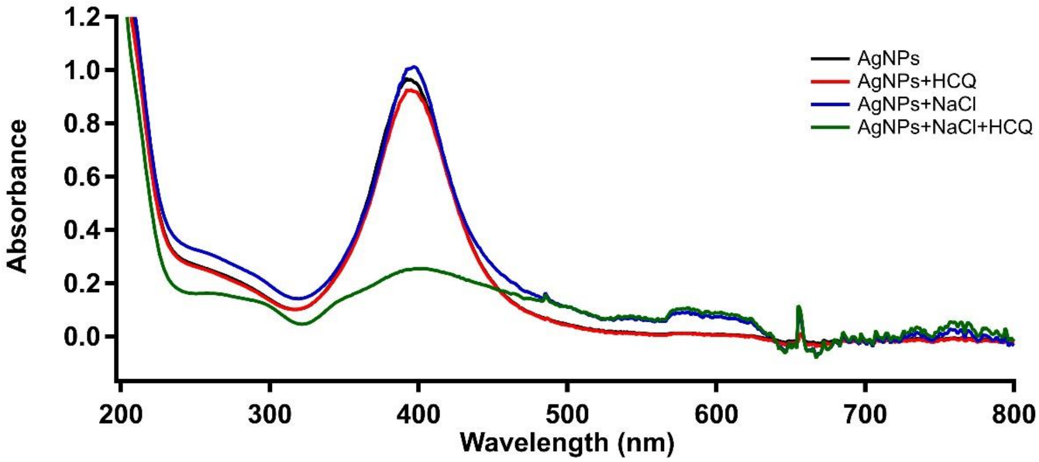

Figure 2: UV-Vis spectra of Cit-AgNPs, Cit-AgNPs+NaCl and Cit-AgNPs+NaCl+HCQ at room temperature.

The interactions of HCQ with Cit-AgNPs were also apparent to the naked eye especially in the presence of NaCl as they could be visualized via the color change from yellow to colorless upon addition of HCQ onto Cit+AgNPs+NaCl (Figure 3) sample. The color of AgNPs was yellowish-gray (the 1st cuvette). The color didn't change upon addition of only HCQ or NaCl (2nd and 3rd cuvettes). It changed to colorless only when HCQ was added onto AgNPs in the presence of NaCl (4th cuvette).

Overall, the changes observed in the color of the solution and the LSPR signal in the presence of NaCl suggested the possible use of Cit-AgNPs in detection of HCQ. Consequently, a detection platform was developed within the context of this thesis using Cit-AgNPs+NaCl+HCQ interactions. In order to develop a sensitive platform, first the conditions that are thought to have a possible effect on the Cit-AgNPs+NaCl+HCQ interactions such as NaCl concentration, incubation time and temperature were optimized.

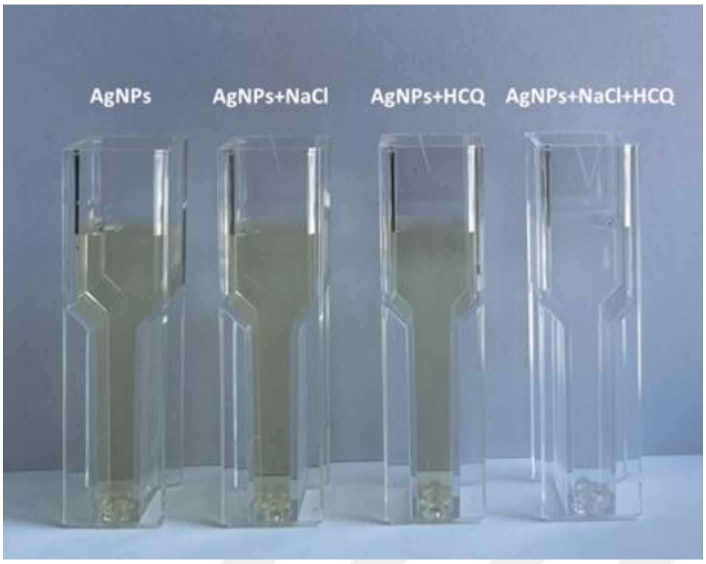

Figure 3: Photographs of Cit-AgNPs, Cit-AgNPs+NaCl, Cit-AgNPs+HCQ and Cit-AgNPs+NaCl+HCQ after 5 min of incubation at room temperature.

3.2 Optimization of the Factors Affecting HCQ Detection

3.2.1 The Effect of NaCl Concentration

Our initial experiments revealed that the presence of NaCl had a crucial effect on the LSPR signal of Cit-AgNPs and thus the interactions of HCQ with Cit-AgNPs. Therefore, the effect of the concentration of NaCl on the detection platform was assessed first.

In order to reveal the effect of NaCl concentration on Cit-AgNPs-HCQ interactions, samples with NaCl concentrations in the range of 0.3-66.7 mM were prepared. To obtain samples with varying NaCl concentrations, different volumes of 1.0 M NaCl (1.0-200.0 µL) and H_2O (required to complete the total volume to 3000.0 µL) were added onto AgNPs solutions (2700.0 µL, ~0.01 mgAg/mL) and mixed thoroughly. UV-Vis spectra were collected for each sample. Then, HCQ (100.0 µL from 10.0 µM solution, final concentration: 333.3 nM) was added onto each Cit-AgNPs+NaCl solution. UV-Vis spectra of the samples were collected 10 minutes after HCQ addition in order to allow through AgNP+NaCl+HCQ interactions (Figure 4). The experiments were performed in triplicate.

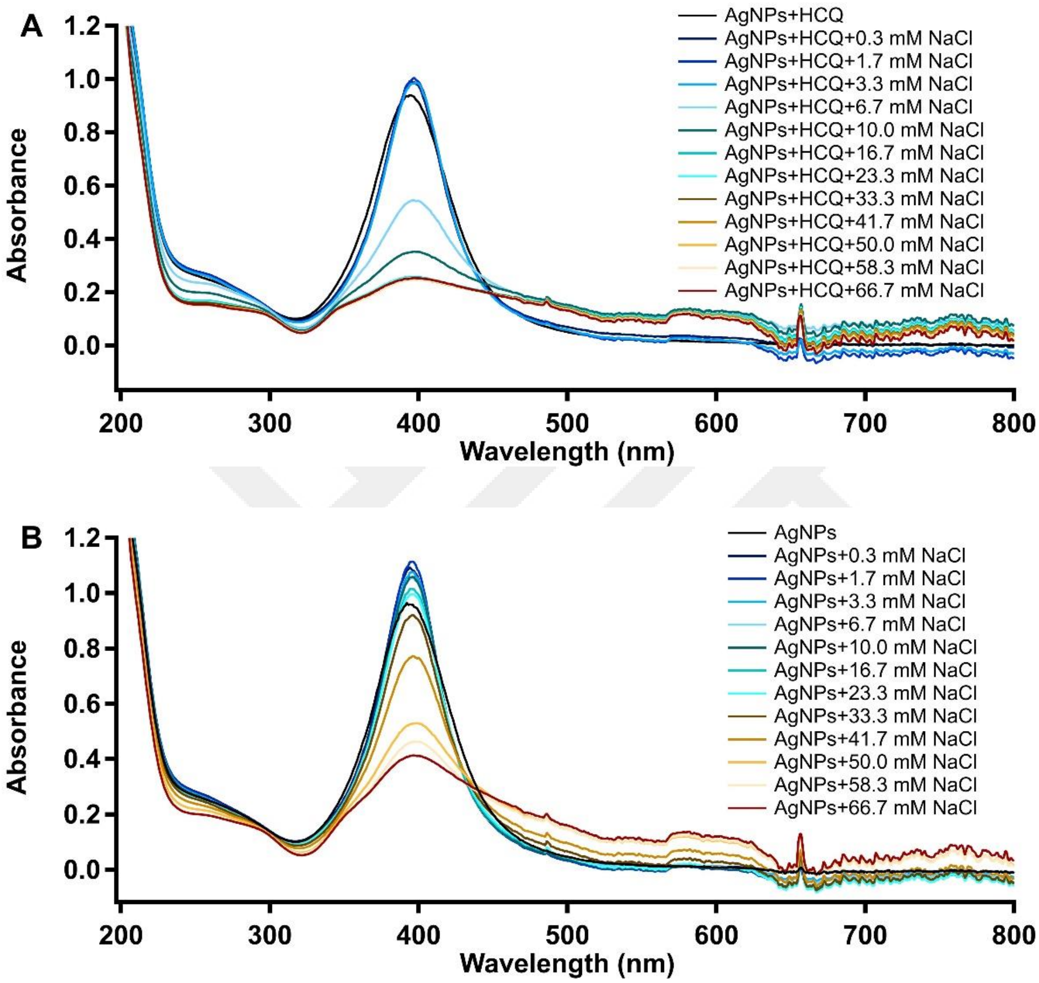

Figure 4: (A) UV-Vis spectra of Cit-AgNPs with increasing NaCl concentration (0.3-66.7 mM) in the presence of HCQ. (B) UV-Vis spectra of Cit-AgNPs with increasing NaCl concentration (0.3-66.7 mM).

Colloidal stability refers to the ability of particles to resist aggregation. It is influenced by solution conditions (such as pH or electrolyte concentration) and the type of capping agents [127]. Any condition that would result in a change in the properties of AgNPs' surface will change the physicochemical properties of AgNPs and could result in aggregation [127]. In the case of Cit-AgNPs, the stability of Cit-

AgNPs in solution depends on the interparticle repulsions arising from the negatively charged citrate ions on the nanoparticles' surface. The repulsions between the particles prevent aggregation of the nanoparticles. As shown with the black colored spectra in Figure 4, in the absence of aggregation the LSPR band gets sharper and its intensity increases [128]. At low concentrations of NaCl, Na^+ ions are attracted by the negatively charged Cit-AgNPs surface and form an electrical double layer which is yet not able to notably decrease the repulsive forces between the particles. At higher concentrations of NaCl, Na^+ ions strongly interact with citrate ions on the surface of the AgNPs [128-132]. As a result, the negative charge on the surface is reduced which causes the weakening of interparticle repulsions, reduced stability of Cit-AgNPs and aggregation. High Na^+ concentrations are also reported to possibly remove citrates from the AgNPs surface [128-132]. The removal of citrate ions from the surface are thought to facilitate the interactions of other analytes present in the medium with AgNPs. Previous studies have reported critical coagulation concentrations of NaCl for Cit-AgNPs in the range of 40-86 mM [128, 130-132]. In this study, we aimed to determine NaCl concentration range which would not cause aggregation in the absence of HCQ and allow the detection of HCQ by facilitating the interactions between HCQ and Cit-AgNPs.

UV-Vis spectra of Cit-AgNPs+NaCl and Cit-AgNPs+NaCl+HCQ samples are given in Figure 4. In order to reveal the apparent effect of changing NaCl concentration (0-66.7 mM) on the system, the absorbances of samples at 395 nm before and after HCQ addition were plotted as shown in Figure 5.

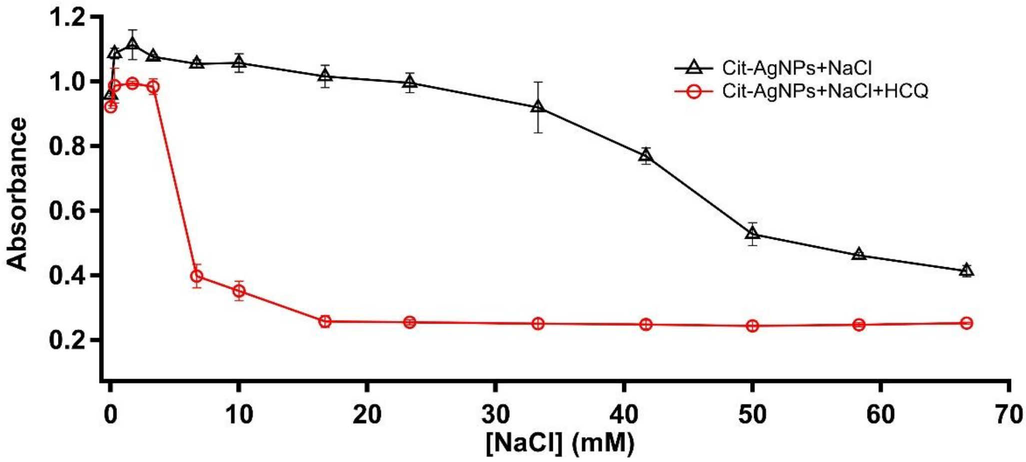

Figure 5: Absorbance values of Cit-AgNPs with varying NaCl concentrations at 395 nm in the absence and presence of 333.3 nM HCQ at room temperature. Error bars represent the SD of three independent measurements.

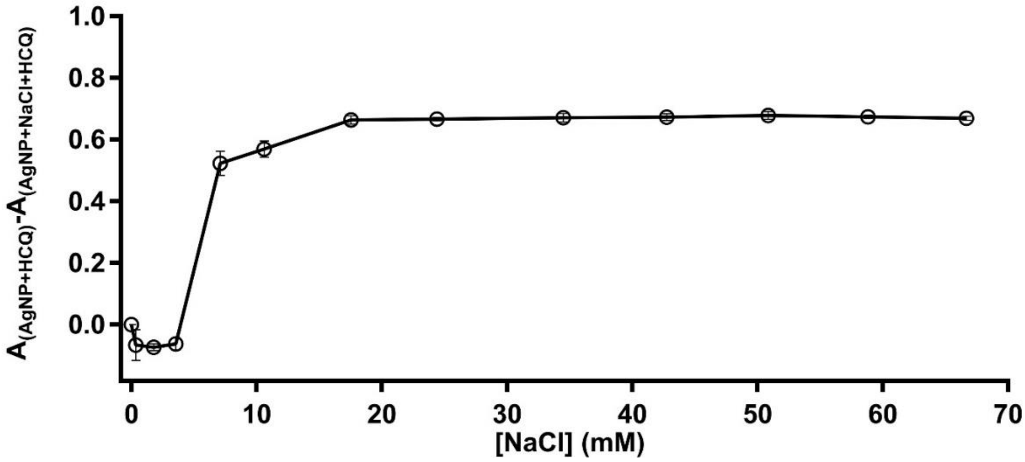

Figure 6: ($A_{(Cit\text{-}AgNPs+HCQ)}$-$A_{(Cit\text{-}AgNPs+NaCl+HCQ)}$) at 395 nm vs [NaCl] graph for Cit-AgNPs-HCQ interactions. Error bars represent the SD of three independent measurements.

Our results revealed that the intensity of the LSPR signal belonging to the Cit-AgNPS+NaCl sample start decrasing significantly around 35.0 mM NaCl, and the decrease was less gradual after about 50 mM NaCl due to the aggregation in the presence of high salt concentration. As mentioned above, such aggregation is expected due to the decreased repulsions between AgNPs and previous studies revealed aggregation of AgNPs in the range of 40-86 mM [128, 130-132]. The aggregation of Cit-AgNPs+NaCl in the presence of HCQ started after addition of 5 mM NaCl, and almost complete aggregation was observed when NaCl concentration exceeded 20.0 mM. Aggregation of Cit-AgNPs in the presence of HCQ was more gradual (Figure 5).

Furthermore, the difference plot is obtained by the absorbance difference of the Cit-AgNPs+HCQ and Cit-AgNPs+NaCl+HCQ samples at 395 nm (Figure 6). Difference plot reveals the effect of NaCl on the aggregation behaviour in the presence of HCQ more explicitly. The aggregation was almost steady after addition of 20.0 mM NaCl. Consequently, by comparing the aggregation Cit-AgNPs in the presence of only NaCl to their aggregation behavior in the presence of both NaCl and HCQ, the optimum NaCl concentration range for HCQ detection was determined to be as 20.0-50.0 mM. Accordingly, 30.0 mM NaCl was used in further experiments. Besides, our results also revealed that the concentration of NaCl was particularly important such that it should be monitored and controlled closely during the development of our detection platform.

3.2.2 The Effect of Incubation Time

Next, the effect of the length of incubation period on the aggregation behavior of Cit-AgNPs in the presence of NaCl and HCQ was assessed. As mentioned above, the presence of HCQ causes the aggregation of Cit-AgNPs in the presence of NaCl, resulting in a decrease in the LSPR signal. To find the optimum length of incubation time that allows for through interactions of Cit-AgNPs with HCQ in the presence of NaCl, the absorbance of the Cit-AgNPs+NaCl+HCQ sample (2810.0 μL Cit-AgNPs+90.0 μL 1.0 M NaCl+100.0 μL 10 μM HCQ) at 395 nm was measured at definite time intervals (at 0.5, 1, 2, 4, 6, 8, 10, 12, 14, 16, 18, 20, 30, 40, 50, 60 minutes) after HCQ addition. The changes in the absorbance with respect to the absorbance of the initial Cit-AgNPs+NaCl solution were calculated for each interval to obtain the ($A_{(Cit\text{-}AgNPs+NaCl)}$-$A_{(Cit\text{-}AgNPs+NaCl+HCQ)}$) vs. time (min) graph in Figure 7.

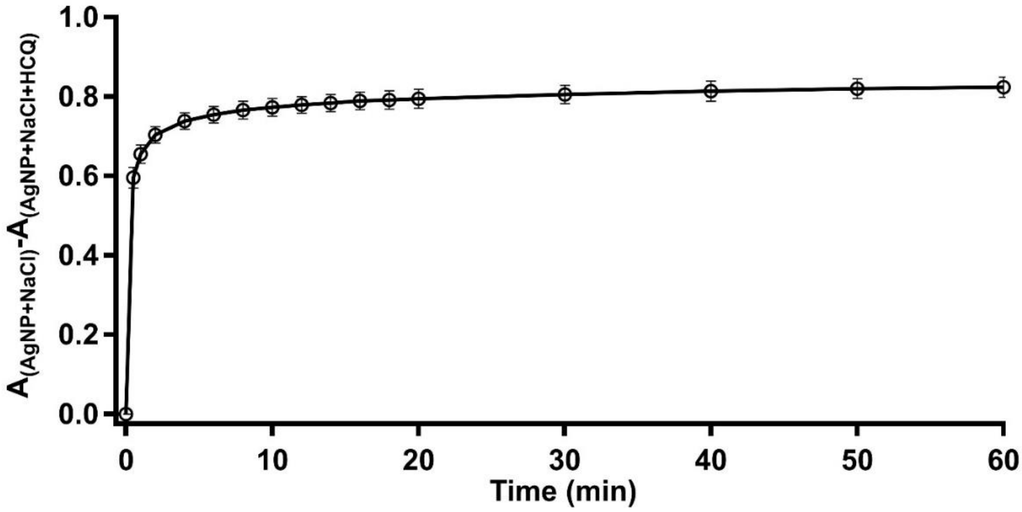

Figure 7: The change in the absorbance at 395 nm with time after 333.3 nM HCQ addition in the presence of 30.0 mM NaCl at room temperature. Error bars represent the SD of three independent measurements.

As displayed in Figure 7, the absorbance was almost steady 5 minutes after the HCQ addition. In order words, the aggregation of Cit-AgNPs+NaCl+HCQ was almost complete after 5 minutes. Since our goal was to develop a simple and fast detection platform for HCQ detection, in the following experiments, UV-Vis spectra were taken 5 minutes after HCQ addition.

3.2.3 The Effect of Temperature

Previous studies, reported agglomeration of Cit-AgNPs with increasing temperature, especially in the long term, possibly due to the increased collisions between the particles [55, 128, 133, 134]. The temperature of Cit-AgNPs' storage conditions has also been shown to have an effect especially on their long term stability (Appendix A). In order to understand the effect of temperature on our detection platform under the optimized conditions, UV-Vis absorbance of Cit-AgNPs at 395 nm in 30.0 mM

NaCl were collected at different temperatures between 15 °C and 75 °C after addition of HCQ (final concentration 333.3 nM) (Figure 8). The absorbance values of Cit-AgNPs at 395 nm in 30.0 mM NaCl in the absence of HCQ were also collected within the same temperature range. As temperature increased, the SPR absorption decreased slightly due to the possible agglomeration of Cit-AgNPs as reported previously [128, 133, 134]. However, the decrease was not that significant and we decided to carry out the following experiments at ambient temperature to take advantage of fast detection and lesser need for temperature regulating instrumentation.

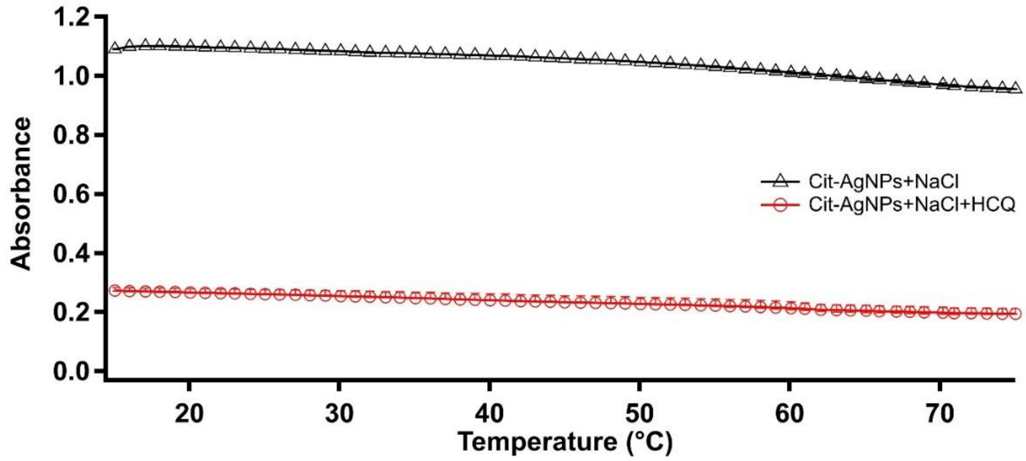

Figure 8: Absorbance vs temperature (°C) graph for Cit-AgNPs+NaCl and Cit-AgNPs+NaCl+HCQ system. Error bars represent the SD of three independent measurements. Note: SD values of Cit-AgNPs+NaCl was very small that they are almost invisible on the graph.

3.3 Characterization

To provide further information for the Cit-AgNPs+NaCl and Cit-AgNPs+NaCl+HCQ interactions, and to explain the mechanism behind our detection platform, TEM images and FTIR spectra of the samples were collected and DLS and zeta potential measurement were performed.

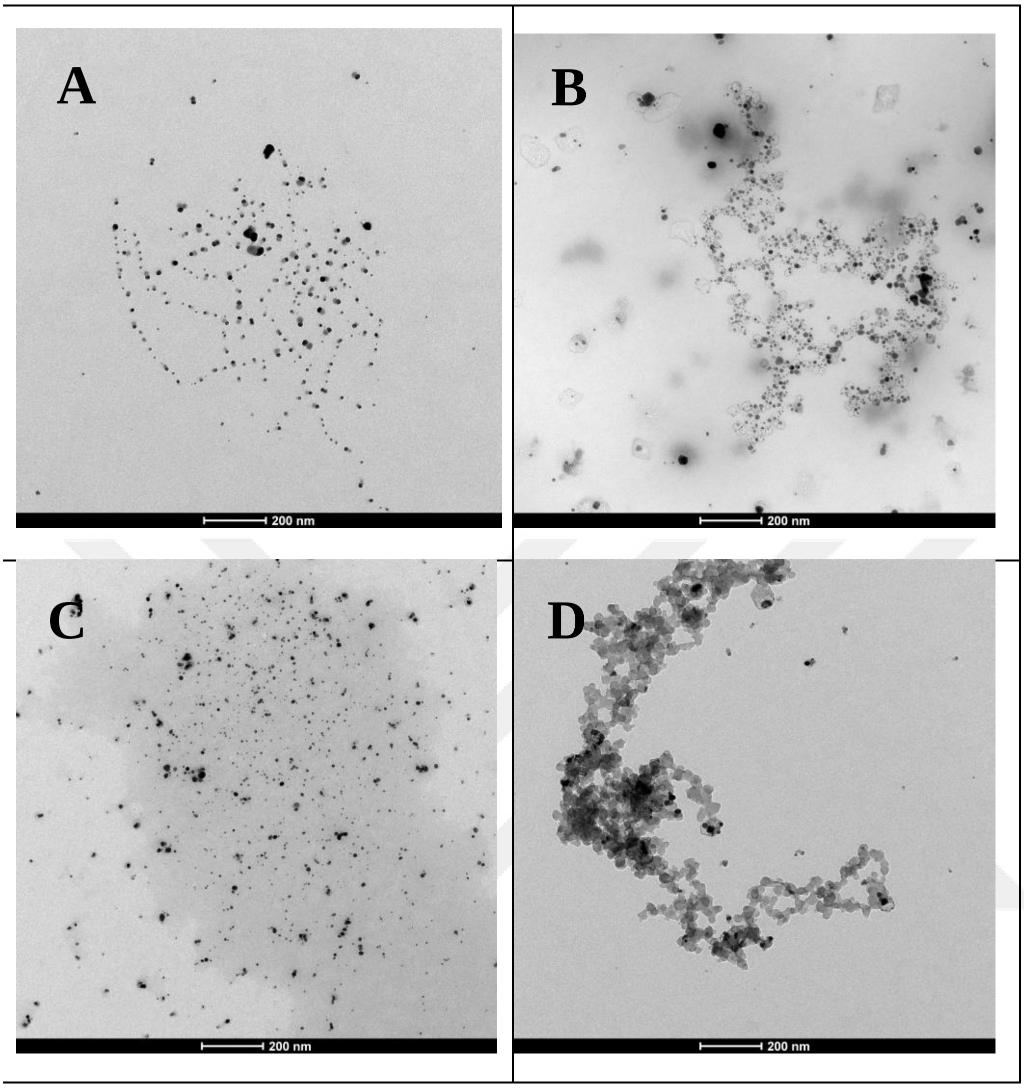

Figure 9: TEM images of (A) Cit-AgNPs, (B) Cit-AgNPs+NaCl, (C) Cit-AgNPs+HCQ and (D) Cit-AgNPs+NaCl+HCQ taken at 200 nm magnification. The samples contained ~0.01 mg Ag/mL AgNPs, 30.0 mM NaCl or 200 nM HCQ.

TEM images revealed that the synthesized Cit-AgNPs had a diameter of around 10 nm (Figure 9A). Nanoparticles were distanced from each other in the pure solution due to the repulsions which arose from negatively charged citrates on the AgNPs surface. They began to be attracted to each other when the repulsion forces were disturbed by the presence of NaCl which, at high concentrations, neutralizes the negative surface charge and removes the negatively charged capping agents from the surface of nanoparticle [128-132]. As can be seen from the images, the optimized NaCl concentration, 30.0 mM, was not sufficiently high either to neutralize citrate ions completely or aggregate Cit-AgNPs. As expected, the sizes of Cit-AgNPs did not significantly change in the presence of 30.0 mM NaCl. Formation of a salt layer could be observed in several particles (Figure 9B). TEM images of Cit-AgNPs+HCQ samples were also collected as a control. In an agreement with or UV-Vis results, no aggregation was observed only in the presence of HCQ without NaCl (Figure 9C). When HCQ is added to Cit-AgNPs in 30.0 mM NaCl, nanoparticles formed aggregates as expected based on our UV-Vis results (Figure 9D). This is again probably a result of NaCl addition at a concentration which will allow the partial neutralization of the citrate ions from the surface and the possible interactions of HCQ with Cit-AgNPs, contributing to a decrease in repulsion between the nanoparticles.

To explain the interactions and the aggregation mechanism clearly, DLS and zeta-potential measurements were performed (Figure 10 and Figure 11). The average sizes of Cit-AgNPS, Cit-AgNPs in the presence of 30.0 mM NaCl and Cit-AgNPs with 300.0 nM HCQ in the presence of 30.0 mM NaCl were obtained (Table 1).

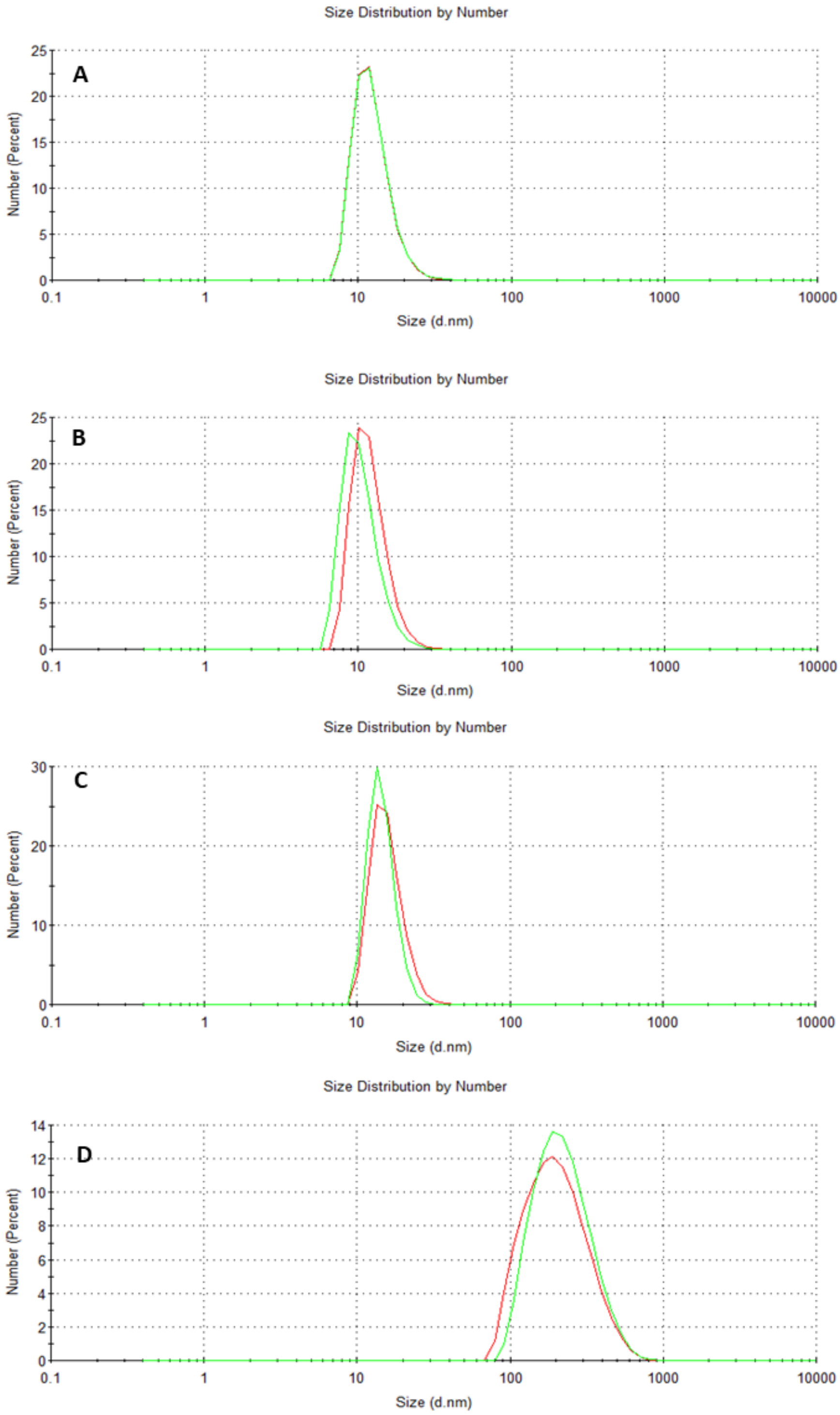

Figure 10: DLS size distributions of (A) Cit-AgNPs, (B) Cit-AgNPs+HCQ, (C) Cit-AgNPs+NaCl and (D) Cit-AgNPs+NaCl+HCQ. The samples contained ~0.01 mg Ag/mL AgNPs, 30.0 mM NaCl or 300 nM HCQ. (DLS measurements were performed twice for each sample and both size distribution curves for each sample were reported in the graph belonging to that sample.)

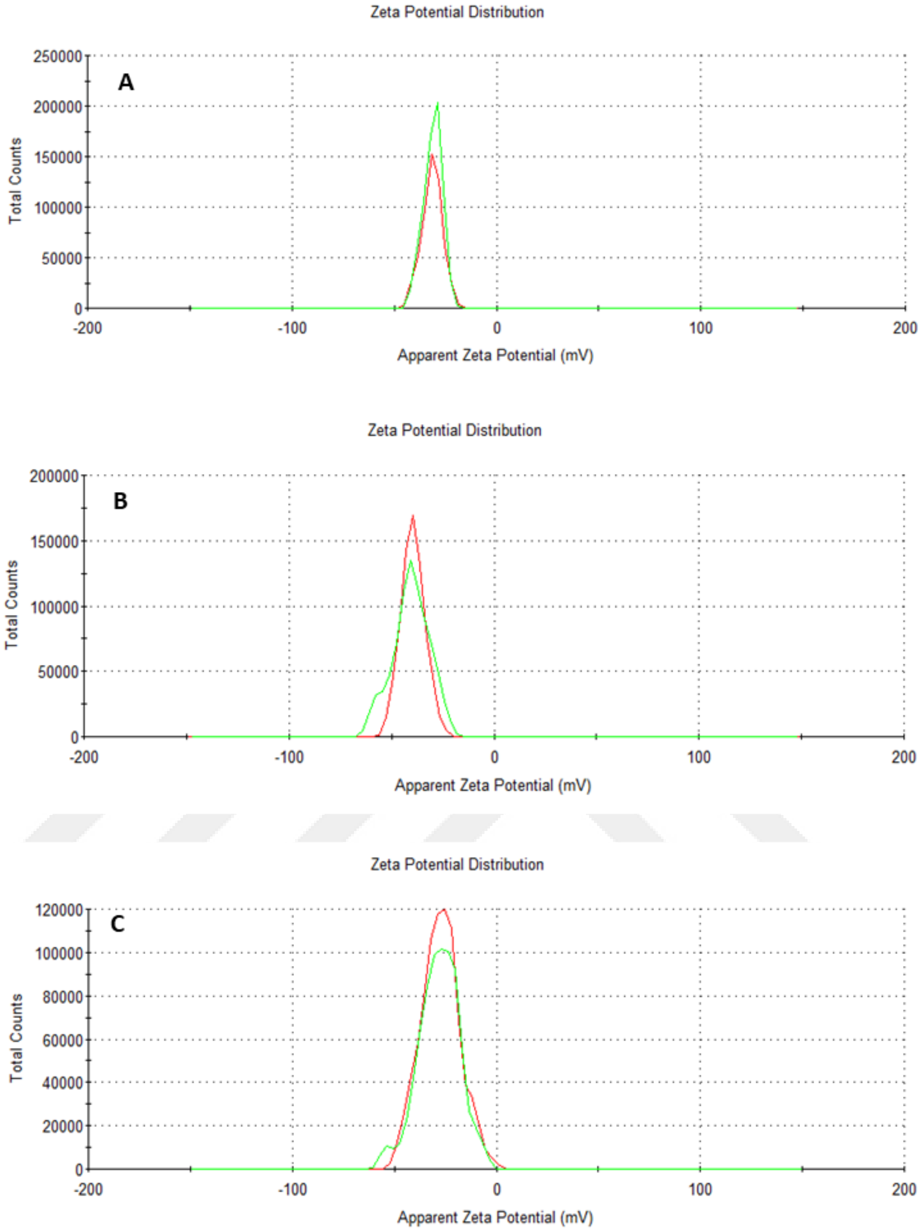

Figure 11: Zeta-potentials of (A) Cit-AgNPs, (B) Cit-AgNPs+HCQ and (C) Cit-AgNPs+NaCl. s samples contained ~0.01 mg Ag/mL AgNPs, 30.0 mM NaCl or 300 nM HCQ.

Table 1: Average sizes and zeta potential values of the samples.

	DLS Size by Number $\pm$ *SD (nm)*	*Zeta Potential*$\pm$ *SD (mV)*
Cit-AgNPs	12.46$\pm$0.02	-31.3$\pm$0.3
Cit-AgNPs+HCQ	11.27$\pm$1.06	-27.8$\pm$0.4
Cit-AgNPs+NaCl	15.15$\pm$0.91	-40.0$\pm$0.6
Cit-AgNPs+NaCl+ HCQ	226.30$\pm$12.16	-

The average size of Cit-AgNPs was found to be 12.46$\pm$0.02 nm (Figure 10A), which is in a good agreement with UV-Vis spectrum and TEM images [51, 118, 122]. The size of the particles did not change upon addition of only HCQ onto the Cit-AgNPs (Figure 10B). Addition of NaCl increased the average size of Cit-AgNPs non-significantly and slightly from 12.46 nm to 15.15 nm (Figure 10C). Here, the slight change in the size depend on the formation of a thin electrical double layer with the interactions of Na^+ ions and citrate ions on the nanoparticle's surface. DLS results also revealed a remarkable increase in average size of Cit-AgNPs after addition of HCQ in the presence of NaCl under the optimized conditions (Figure 10D). In this case, HCQ which is in protonated form might have replaced or neutralized the citrate ions on the surface partially, resulting in a decrease in the repulsive interactions between the nanoparticles [135-137]. Both probabilities are supported by TEM images (Figure 9). As it will be explained in the selectivity section, the aggregation is triggered by the presence of HCQ which can be a result of its distinct structural features from the other drugs and quinolones. Negative zeta potential values implied that surface charge of the particles arises from the deprotonated carboxylic groups of capping agent, citrate ions (Figure 10). There was not a significant change in zeta potential values upon the addition of NaCl or HCQ which indicates perseverance of the surface charge of Cit-AgNPs. A zeta potential value of -31.3±0.3 was measured for Cit-AgNPs (Figure 11A). The zeta potential value increased slightly to -27.8±0.4 upon addition of only HCQ into Cit-AgNPs solution (Figure 11B). The results of zeta potential measurements for AgNPs+NaCl sample (containing 0.03 M NaCl electrolyte solutions) were -40.0 mV suggesting that the AgNPs may be covered with AgCl (Figure 11C). Since pure AgCl particles have a high negative zeta potential (-57 mV) [138], any significant change in zeta potential after the addition of NaCl to Cit-AgNPs samples with a non-bimodal distribution of zeta potential would indicate that some of the AgNPs are coated with AgCl. We repeated the zeta potential measurements several times and found that the average zeta potential of -30 to -35 mV reappeared in the sample under the same measurement conditions (data not shown). However, we believe that the obtained zeta potentials are similar to those measured in previous studies and support the hypothesis that the AgNPs are covered with AgCl [139, 140]. This AgCl coating may be due to the direct precipitation of AgCl on the surface of the oxidized AgNPs, which form a more or less uniform layer, but it may also be the result of the sorption of small AgCl nuclei that initially form in solution. The growth mechanism of an AgCl structure on the surface of AgNPs is difficult to characterize on nanoparticles for the moment and is not within the scope of this thesis. However, we believe that the consistency of the obtained results in the probe solution and upon the addition of the target analyte supports our proposed mechanism and ensures the applicability of the developed probe for HCQ detection.

The zeta potential value for Cit-AgNPs+NaCl+HCQ sample could not be obtained since the conductivity exceeded the measurement limits of instrumentation in the presence of 300.0 nM HCQ.

ATR-FTIR Spectra of Cit-AgNPs in the absence (red spectrum) and presence of HCQ along with the ATR-FTIR spectra of only the target analyte (HCQ, navy blue spectrum) as well as the probe solution (AgNPs+NaCl) (black spectrum) in the range 4000–500 cm^{-1} are presented in Figure 12. From the spectrum of pure HCQ, it can be seen that the sharp peaks at about 1615 cm^{-1} and 1460 cm^{-1} correspond to aromatic C=C stretching vibrations, while the peaks at 2920-2980 cm^{-1} confirm the aromatic C-H stretching vibrations in the original HCQ sample. Moreover, the C-Cl stretching vibration was observed at around 1050 cm^{-1}, while the C-N bending frequency is seen at 1110 cm^{-1}. In the FTIR spectra of Cit-AgNPs and AgNPs+NaCl samples, the characteristic bands at 1400-1420 cm^{-1} correspond to the symmetric stretching of -

COO$^-$ and at 1590-1600 cm^{-1} for the antisymmetric stretching of -COO$^-$ of the citrate molecules [141-144] are visible, confirming the surface capping of AgNPs with citrate ions. As can be seen, the addition of NaCl has no remarkable effect on the surface of the silver nanoparticles in terms of capping with citrate ions, which is in good agreement with the results of the zeta potential measurements.

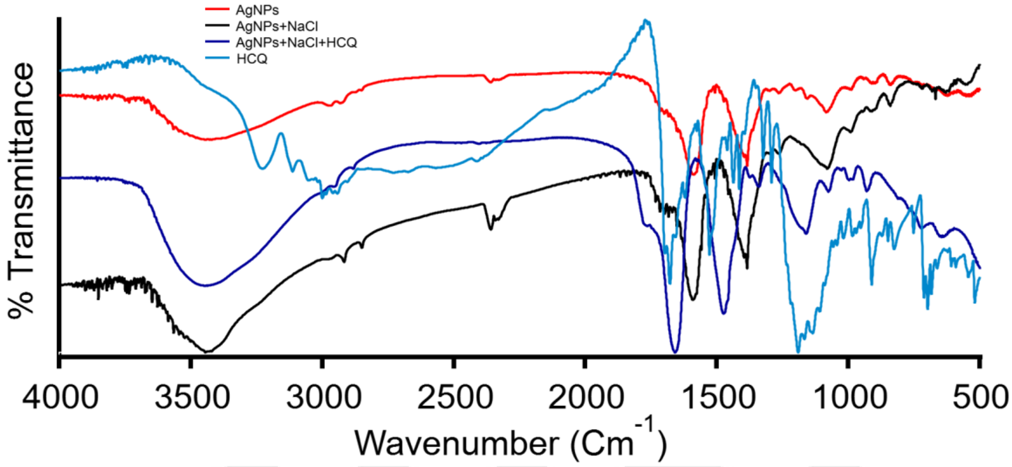

Figure 12: ATR-FTIR spectra of HCQ (navy blue line), Cit-AgNPs (black line), Cit-AgNPs+NaCl (red line) and the probe in the presence of 200.0 nM HCQ (Cit-AgNPs+NaCl+HCQ, blue line).

The pattern of the fingerprint region of the Cit-AgNPs+NaCl+HCQ (navy blue spectrum) sample appeared to be different from that of the pure HCQ (blue spectrum). The FTIR spectrum of Cit-AgNPs+NaCl+HCQ was rather very similar to the FTIR spectrum of the Cit-AgNPs (red spectrum) and Cit-AgNPs+NaCl (black spectrum) samples. We only observed some broadening as well as minor shifts in peak positions in the 1400-1600 cm^{-1} range, making it difficult to follow the changes in the spectra. Moreover, we did not observe any significant evidence of the disappearance of citrate ions in the 1400-1600 cm^{-1} region (the region attributed to asymmetric C=O stretching in COO$^-$ and symmetric C=O stretching of carboxylate ion of citrate) in the FTIR spectra recorded. This might be due to the low concentration of HCQ at our optimized condition during method development, which could be assessed in further studies.

3.4 Selectivity

The selectivity of the developed probe for HCQ was determined under the optimized conditions. For these studies, quinolines that have similar structure to HCQ or the ones that were used together with HCQ, especially during the initial phase of COVID-19 pandemic such as acetyl salicylic acid (ASA), favipiravir (FAV), ivermectin (IVM), ritonavir (RTV) and lopinavir (LPV) [145] were selected. The structures of the small molecules used in selectivity studies are given in Figure 13.

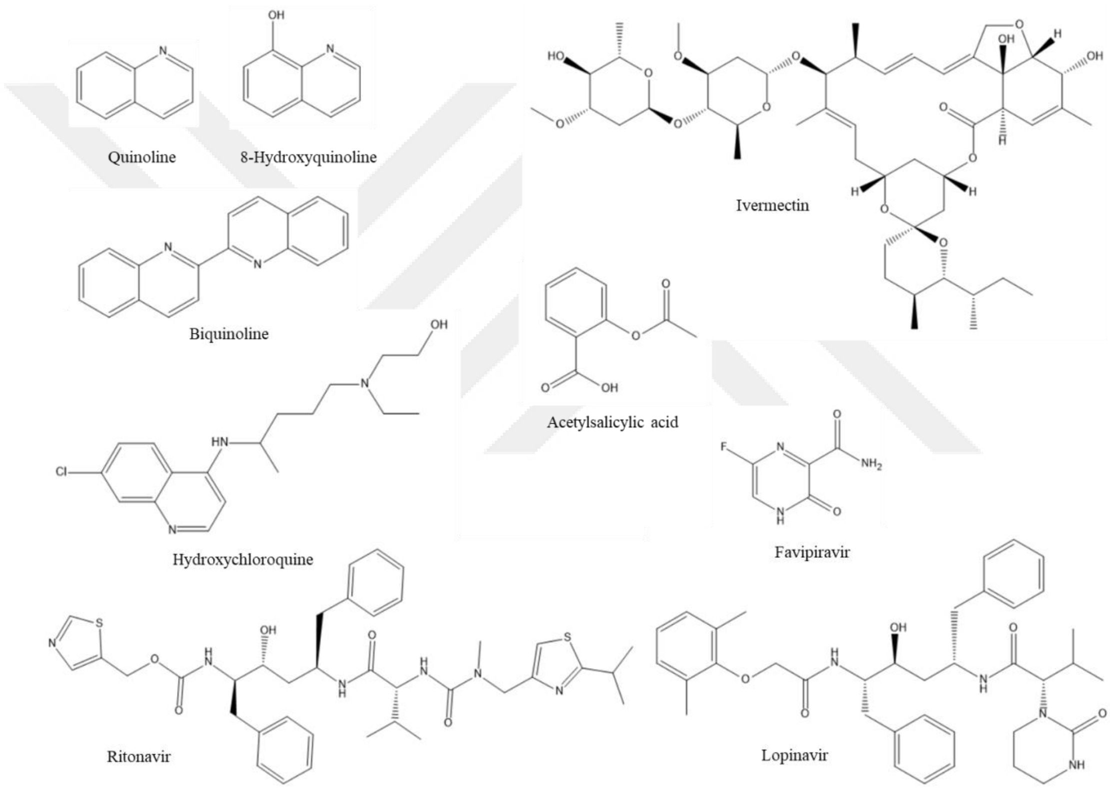

Figure 13: Molecular structures of the quinoline derivatives and the drugs used in selectivity studies.

First, Cit-AgNPs samples containing drugs and quinoline derivatives were prepared under the previously optimized conditions, and the UV-Vis spectra of the samples were collected (Figure 14). No change in the LSPR band was observed upon the addition of the other small molecules to Cit-AgNPs. In other words, none of the other small molecules were able cause the aggregation of the Cit-AgNPs as HCQ (blue spectrum). The degree of aggregation could also be observed by examining the color change in the cuvettes (Figure 15). Only the color of the solution in the cuvette with HCQ changed to colorless from yellow (3rd cuvette from left). All the other cuvettes appeared yellow to the eye. To further elaborate on the selectivity of our detection platform, samples containing the mixtures of only drugs, only quinoline derivatives and both drugs and quinolines were prepared with and without HCQ. The final concentration of each drug and quinoline derivative was 200.0 nM in all experiments UV-Vis spectra for these samples are given in Figure 16. The samples containing HCQ exhibited a significant decrease in the absorbance at 395 nm (solid line spectra, except the black spectrum) while the samples with only drugs or quinolines (dashed line spectra) did not yield any decrease in the absorbance at 395 nm, confirming the inability of the other molecules to cause any aggregation. Overall, our data shows that Cit-AgNPs are highly selective to HCQ in the presence of NaCl under given conditions.

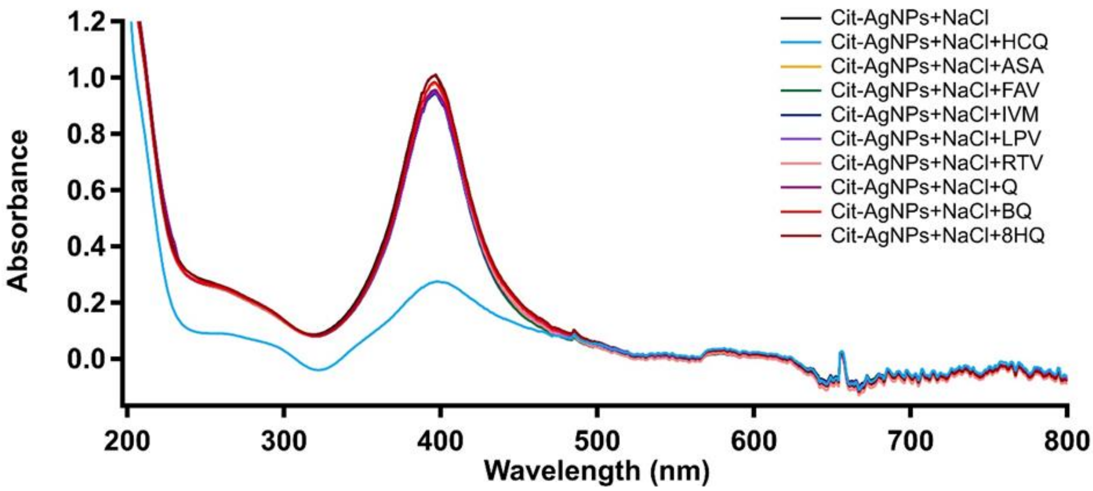

Figure 14: UV-Vis spectra of Cit-AgNPs with different drugs and quinoline derivatives (200 nM each) in the presence of 30.0 mM NaCl.

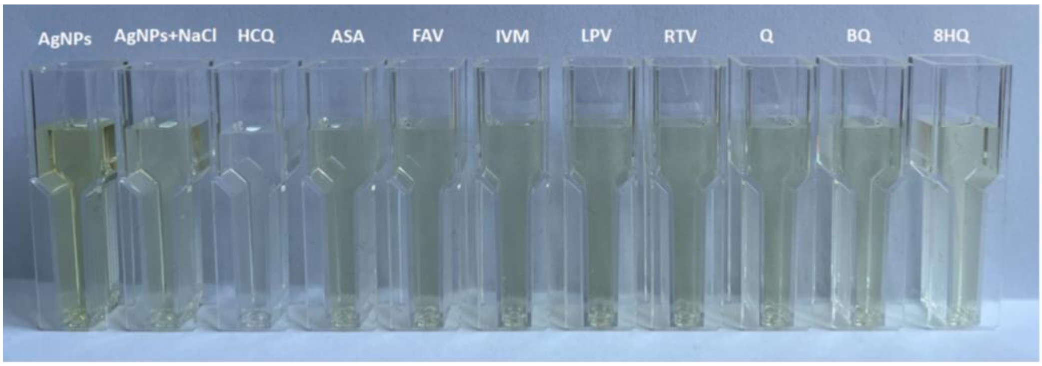

Figure 15: Photographs of Cit-AgNPs with different drugs and quinoline derivatives (200 nM each) in the presence of 30.0 mM NaCl.

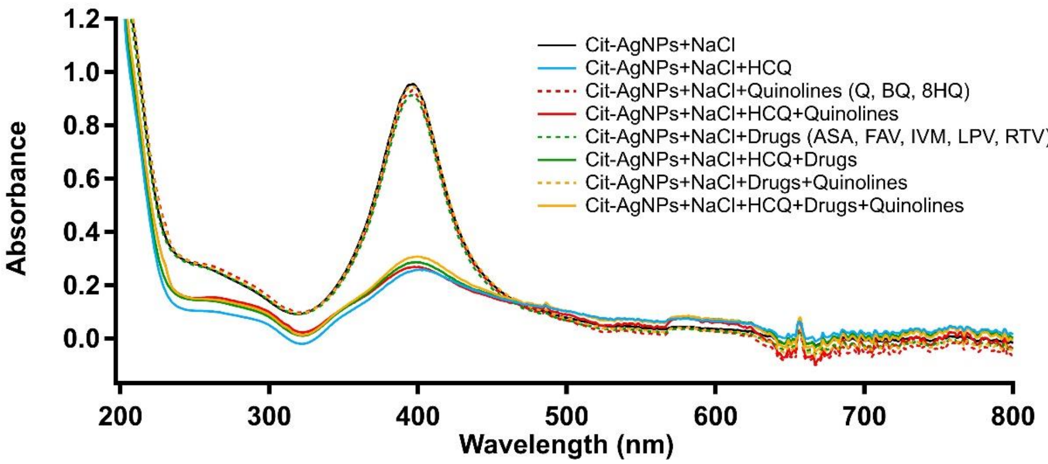

Figure 16: UV-Vis spectra of Cit-AgNPs with drug and quinoline mixtures (200 nM each) in the presence of 30.0 mM NaCl.

When the molecular structures of the quinolines and the drugs were compared, the side chain of HCQ might plausibly play a role in the selective interactions of HCQ with Cit-AgNPs. Recently, Morad et al. investigated the interactions of HCQ with noble nanoparticles including AgNPs via computational studies [146]. They reported that, the nitrogen of the pyridine ring and oxygen of the hydroxyl group in the side chain have higher affinity to nanoparticles among other groups. The have shown that the interactions of HCQ with AgNPs occur through these groups. Here, even though the quinolines have the nitrogen in the ring, they do lack the hydroxide group on the side chain that HCQ has. In addition, HCQ is reported to have three pK_a values of 4.0, 8.3 and 9.7 [135]. And, recently Martinez reported the electron distribution of HCQ in nonprotonated, hemiprotonated and protonated forms. Under physiological conditions, HCQ is expected to be protonated through its amine groups. The oxygen atom of the hydroxyl group is calculated to be partially negatively charged in the same study [147]. It is highly possible that the interactions between the positively charged nitrogen atoms and the hydroxyl group, with relatively flexible side chain might be contributing to the increased aggregation even between different AgNPs compared to the other drugs. All other examined compounds have no or few short single bond chains or side chains in their ring systems. However, this needs to be proven via further studies.

3.5 Sensitivity Studies

To investigate the Cit-AgNPs' sensitivity towards HCQ, probe solution which was prepared by mixing 2760.0 μL Cit-AgNPs and 90.0 μL NaCl (1.0 M) and was titrated with 10.0 μM HCQ solution (5.0 μL portions in each addition, 0.0 (0 nM) to 150.0 μL (500 nM). The absorbance at 395 nm decreased gradually with the increasing concentration of HCQ during the titration (Figure 17). Then, the change caused by each 5.0 μL addition of HCQ in the absorbance with respect to the absorbance of initial Cit-AgNPs+NaCl solution was calculated and the calibration curve for the method, ($A_{(Cit\text{-}AgNPs+NaCl)}$-$A_{(Cit\text{-}AgNPs+NaCl+HCQ)}$) vs. [HCQ], was plotted (Figure 18).

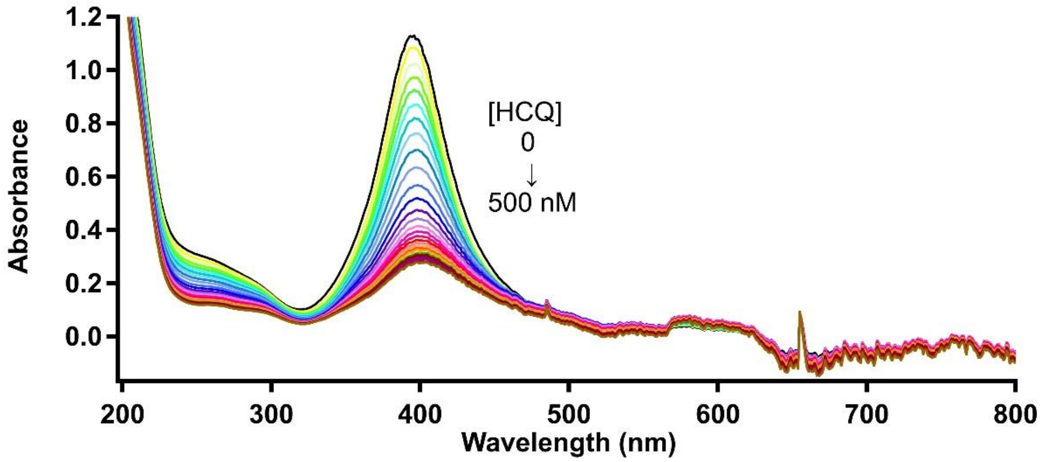

Figure 17: UV-Vis spectra of Cit-AgNPs containing 30.0 mM NaCl with increasing concentrations of HCQ from 0 to 500 nM at room temperature. The intensity of LSPR signal gradually decreases with increasing HCQ concentration.

The curve exhibited a LDR between 18.0-240.0 nM. The LOD was calculated as 9.2 nM which is comparable with the results from previous studies [103-107, 111-116]. The relation of HCQ concentration and LSPR change in the linear range is given in the Equation 3-1:

$$y = 0.0033x - 0.0175, \text{ with } R^2 = 0.9977 \text{ (Eq. 3-1)}$$

The equation is converted to the form below (Eq. 3-2) in order to calculate HCQ concentration by using the LSPR change:

$$[HCQ] = (\Delta A+0.0175)/0.0033 \text{ (Eq. 3-2)}$$

[HCQ]: Final concentration of HCQ

ΔA: The change in absorbance at 395 nm, $A_{(Cit\text{-}AgNPs+NaCl)}-A_{(Cit\text{-}AgNPs+NaCl+HCQ)}$

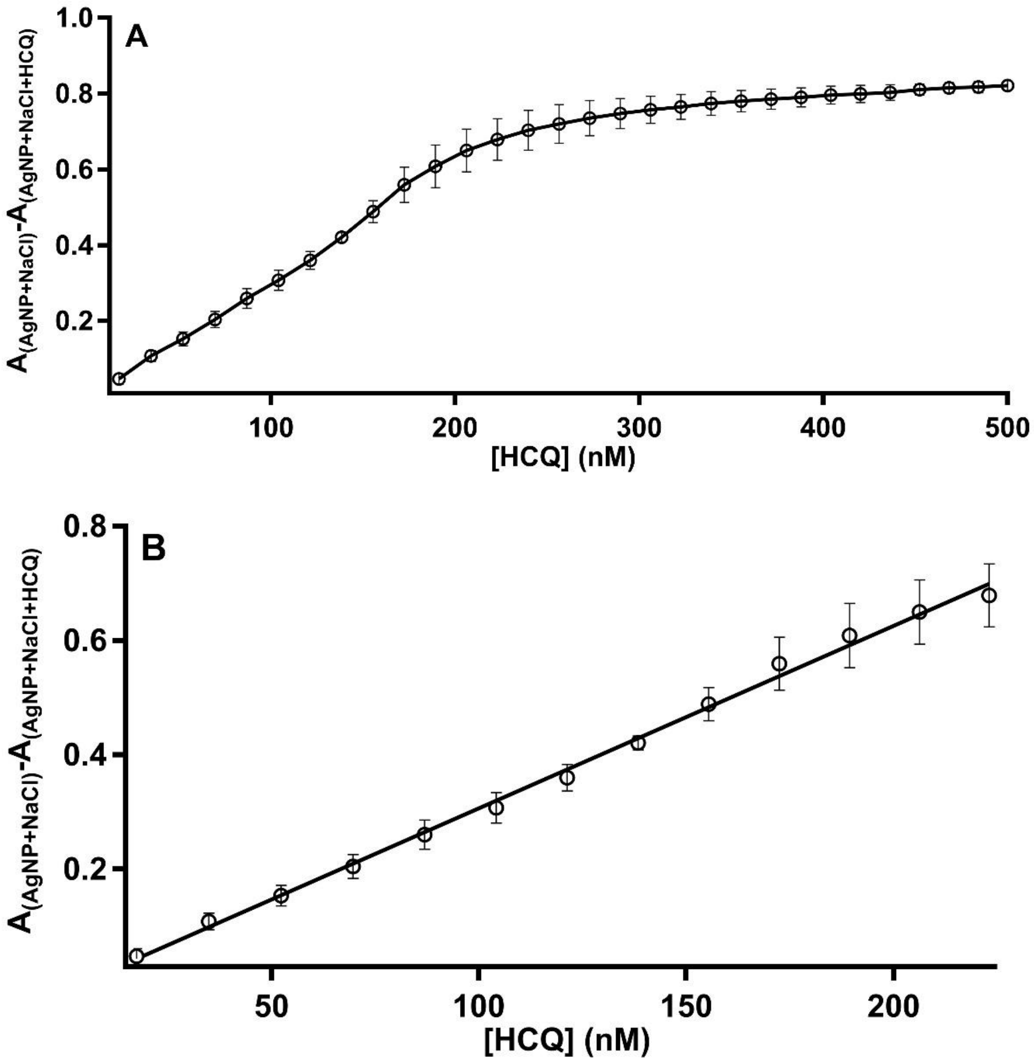

Figure 18: (A) Calibration curve for Cit-AgNPs+NaCl+HCQ system (30.0 mM NaCl, 0.0-500.0 nM final HCQ concentration). (B) The linear range of the calibration curve with the linear regression line.

3.6 Mechanism of Action

The proposed mechanism of action of the developed colorimetric method is illustrated in Scheme 1. UV-Vis studies and TEM images implied the aggregation of AgNPs whereas DLS measurements showed that size of the Cit-AgNPs drastically increased in the presence of HCQ. As mentioned earlier, citrate ions on the surface of the particles bear a negative charge and provide stability to Cit-AgNPs causing repulsion between particles. With increasing concentration of NaCl, Na^+ ions decrease electrostatic repulsion between AgNPs. Once the stability is disturbed, Cit-AgNPs start to form aggregates as reported in the previous studies [127-132], and increasing concentration of NaCl causes aggregation of AgNPs which is consistent with our results. Here, HCQ also plays an essential role in the aggregation process according to the results of the selectivity experiments. It should be noted that, as mentioned earlier, Cit-AgNPs do not aggregate in 30.0 mM NaCl in the absence of HCQ. The presence of other drugs, even the presence of other quinoline derivatives was not able to induce aggregation, which clearly points the importance of the structure of HCQ. Compared to the other molecules HCQ has relatively long and flexible side chain. Other drugs and quinoline derivatives have more rigid molecular structures. It is probable that the side chains of HCQ involve in aggregation process. In their computational studies, Morad et al. reported that HCQ was able to coat onto the AgNPs using nitrogen and oxygen atoms in its side chain [146]. HCQ molecules interacting with the surface of different Cit-AgNPs might also be interacting with each other via van der Waals interactions. Previous studies showed the possible replacement of citrate ions from the AgNPs via ligands or analytes [52, 54, 61-63, 69, 74]. However, further proof is required to make definitive conclusions.

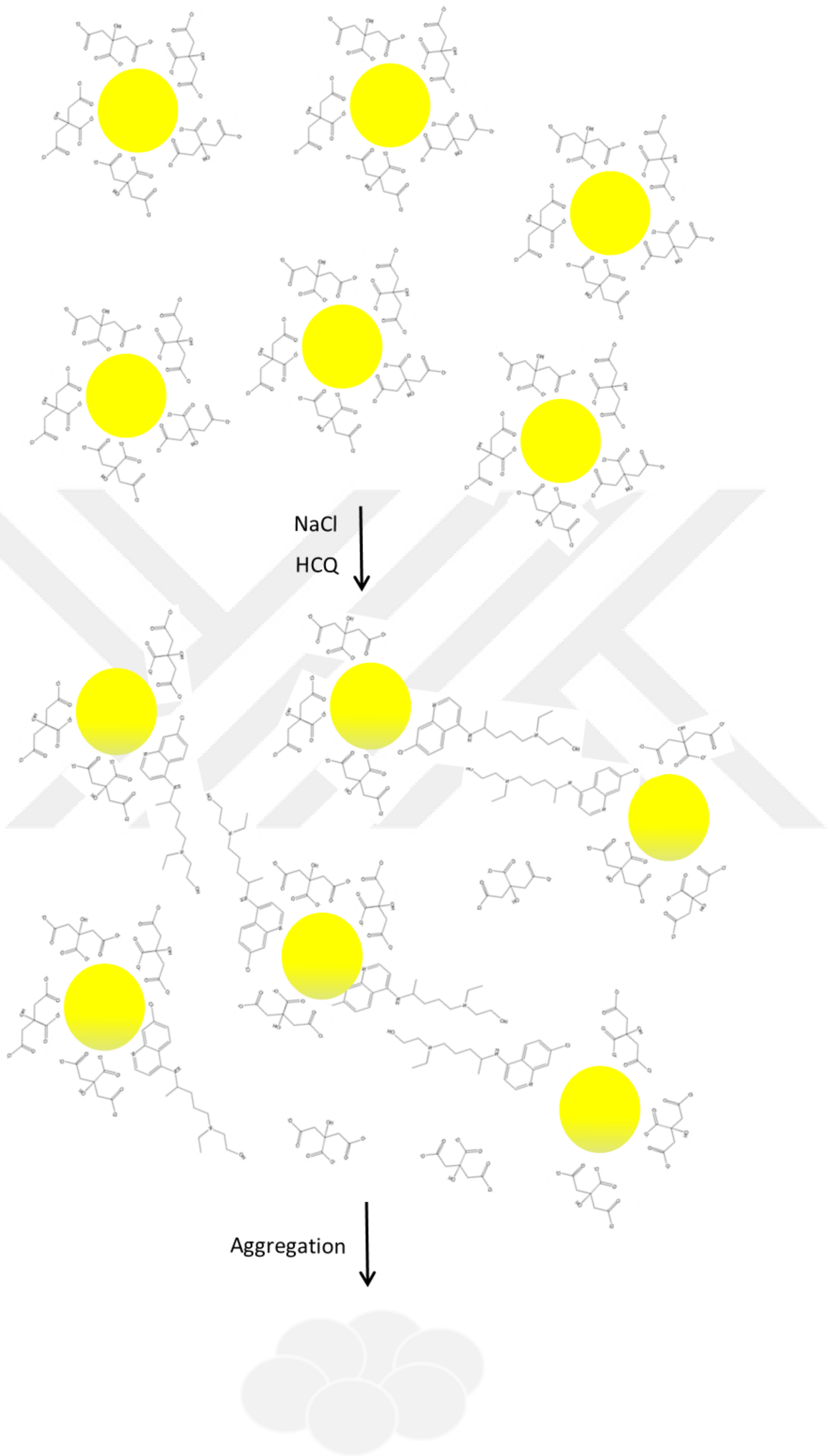

Figure 19: Schematic representation of the mechanism of the proposed Cit-AgNPs-HCQ probe.

3.7 Application of the Method

After investigating and optimizing the factors affecting HCQ detection by Cit-AgNPs in the presence of NaCl, these conditions were applied to detect HCQ in human urine samples. %40-50 of administrated HCQ is excreted from the body via urination [87, 88] which makes urine a preferable medium for HCQ testing. Urine analysis has also the advantage of providing a large volume of samples meaning high quantities of HCQ. In addition, it has the advantage of being a non-invasive technique. The substances present in urine are also relatively stable when frozen and can be stored for a relatively long time. Urine mainly consists of water, urea, creatinine, proteins, inorganic salts, oligosaccharides, and glycosaminoglycans and has a pH of 4.5–8.0 [123, 148].

In experiments dealing with biological samples, the major causes of interference are salts, large molecules such as proteins and buffer system. Those can be altered by dilution, protein precipitation or using a buffer with the desired pH [123-125]. Since the purpose of this study is to develop a less laborious and rapid detection method and the developed method is highly selective to HCQ, we decided to perform dilutions to find a favorable dilution factor for urine samples. Dilution plays and important role in reducing the matrix interferences. However, excess dilution may lead an extreme decrease in analyte concentration. It is crucial to determine a dilution factor which will provide efficient detection with minor interferences. After trial and error through several experiments, dilution of 1:100 was chosen to use in spiking experiments.

In spiking experiments, first the urine samples were filtered and centrifuged (10000 rpm, 20 min) to remove insoluble residues. To reduce interferences arising from proteins, charged large molecules and excess salt, urine samples were diluted in a 1:100 ratio with H_2O. Then, working urine samples with a total volume of 1000.0 μL were prepared by mixing diluted urine and different volumes of HCQ stock solution to obtain urine samples with HCQ concentrations of 1.5, 3.6 and 7.2 μM. Samples for UV-Vis measurements were prepared with 90.0 μL 1.0 mM NaCl and

2810.0 µL Cit-AgNPs and adding 100.0 µL of the diluted urine samples spiked with HCQ which provided samples with final HCQ concentrations of 50.0, 120.0 and 240.0 nM, respectively. UV spectra were taken for each sample before and after HCQ spiked urine addition and absorbance values at 395 nm were recorded. The change in the absorbance was used for calculating HCQ concentrations in the samples by using the equation obtained from the sensitivity graph,

$$[HCQ] = (\Delta A+0.0175)/0.0033 \text{ (Eq. 3-2).}$$

Relative recoveries (Recovery %) calculated from the ratio of the measured concentrations to the theoretical concentrations and relative standard deviations (RSD) are given in Table 2.

Table 2: The obtained recovery and RSD percentages of HCQ in spiked urine samples.

Sample Number	*Spiked HCQ Concentration (nM)*	*Mean Recovery ± SD%*	*RSD%*
1	50.0	93.1 ± 5.4	5.8
	120.0	95.5 ± 1.5	1.6
	240.0	98.2 ± 1.5	1.5
2	50.0	92.9 ± 4.4	4.8
	120.0	87.3 ± 3.5	4.0
	240.0	96.6 ± 3.8	3.9
3	50.0	92.9 ± 5.8	6.2
	120.0	86.9 ± 3.0	3.4
	240.0	94.8 ± 5.1	5.4

CHAPTER 4

CONCLUSION

Development of detection platforms for sensitive HCQ detection have accelerated especially in the last couple of years mainly due to its increased manufacturing and use [107, 112-116, 92-96]. Here, a new simple, fast, cost-effective colorimetric method was developed for HCQ detection based on the change in LSPR signal of Cit-AgNPs upon the interaction of Cit-AgNPs with HCQ in the presence of NaCl. To our knowledge, this is the first platform for colorimetric detection of HCQ based on the aggregation behavior of AgNPs in the presence of NaCl. NaCl concentration was found to be crucial for the aggregation behavior of AgNPs. Since it could lead to aggregation by itself without the analyte at high concentrations, it needed to be closely monitored. Consequently, 30.0 mM NaCl, a concentration which would not induce AgNPs aggregation in the absence of HCQ, along with 5 minutes of incubation time at room temperature were chosen as optimal conditions to develop our platform. Sensitivity studies yielded a calibration curve with LDR of 18.0-240.0 nM and LOD as low as 9.2 nM. Compared to the other methods in the literature, our LDR range and sensitivity can be considered as relatively good. As provided in detail in section 1.4.1, Deroco et. al. reported an LOD of 0.06 µM with an LDR of 0.1 to 1.9 µM using square wave voltammetry (SWV) [113]. Arguelho et al. reported LDR of 2×10^{-5} to 5×10^{-4} M, with a LOD of 11.2 µg/mL (based on our calculations 11.2 µg/mL corresponds to about 26 µM when molecular mass of HCQ sulfate taken as 433.95 g/mol) using a glassy carbon electrode (GCE) [111]. A potentiometric determination of hydroxychloroquine sulfate in pharmaceutical preparations and human urine samples using a new coated graphite electrode yielded a LDR of 9.3×10^{-5}-1.0×10^{-2} M with a LOD of 4.7×10^{-5} M [115]. There were also several reports in the literature on HCQ detection which yielded a letter LOD compared to ours. For instance, Williams et al. and Tett et al. reported LODs of 10 ng/mL and 1 ng/mL, respectively using HPLC coupled with FL [105, 106]. However, compared to ours, their methods were more complex with a need of multiplex extraction steps, different organic solvents and expensive instrumentation. Khoobi et al. reported a LOD of 4.65 nM using glassy carbon electrode and cyclic voltammetry technique [114]. In brief, our developed method was better than many of the detection methods reported so far, yet it was not the most sensitive one. However, it can be considered to be the simplest, fastest and the cheapest so far. As mentioned above, all the other developed platforms based on the use of more laborious and time-consuming sample preparation with high-cost instrumentations. Our method which is straightforward and only requires the use of UV-Vis spectrophotometer, will appeal especially to research groups who lack fully-equipped facilities. Besides, using our method HCQ can be qualitatively monitored by the naked eye based on the color change, which might be used to develop a paper-based sensor in the future.

Another advantage of our developed method is its selectivity. For instance, chromatographic techniques generally require the use of modified columns, which came at expense when similar structures exist in the matrix [107]. In electrochemical methods, mostly the selectivity is determined via separate solution method (SSM) [115], which is more laborious than UV-Vis based methods. And, probably because of that reason neither Deroco et. al. [113] nor Arguelho et. al. [111] reported selectivity using their developed platform. Our selectivity experiments revealed that the method was highly selective to HCQ. Neither the quinolines nor the selected drugs were able to induce aggregation under the selected conditions. The selectivity of the HCQ is thought to be due to the long and flexible chain of HCQ, the hydroxide group on the chain, the presence of N in the ring and its protonation state [135, 146, 147]. Nevertheless, further studies are required to map out the actual mechanism of action of the developed method.

Finally, the applicability of our method was determined via spiking experiments. HCQ was spiked into 100x diluted human urine samples with three final concentrations of 50.0, 120.0 and 240.0 nM. The recovery range, determined to be as 86-98%, demonstrated reasonable accuracy supporting the use of the developed platform in aqueous solutions as urine. The applicability of the method in biological fluids can be determined in future studies.

In conclusion, in comparison to conventional spectrophotometric and sophisticated analytical instruments, the proposed method was found to be simple, sensitive and cost effective for HCQ detection. The lack of the complex matrix elimination procedures and instrumentation, rapid detection, high sensitivity and the stability of Cit-AgNPs provide new opportunities for practical detection of HCQ especially in resource-limited environments.

REFERENCES

1. Boholm, M. (2016). The use and meaning of nano in American English: Towards a systematic description. *Ampersand*, 3, 163-173.
2. Feynman, R. P. (1959, December). Plenty of Room at the Bottom. In APS annual meeting.
3. Taniguchi, N. (1974). On the basic concept of nanotechnology. *Proceeding of the International Conference on Production Engineering (ICPE), Tokyo, 18-23*.
4. Barber, D. J., & Freestone, I. C. (1990). An investigation of the origin of the colour of the Lycurgus Cup by analytical transmission electron microscopy. *Archaeometry*, 32(1), 33-45.
5. Mirguet, C., Roucau, C., & Sciau, P. (2009). Transmission electron microscopy a powerful means to investigate the glazed coating of ancient ceramics. In *Journal of Nano Research*, 8, 141-146.
6. Reibold, M., Paufler, P., Levin, A. A., Kochmann, W., Pätzke, N., & Meyer, D. C. (2006). Carbon nanotubes in an ancient Damascus sabre. *Nature*, 444(7117), 286-286.
7. Bayda, S., Adeel, M., Tuccinardi, T., Cordani, M., & Rizzolio, F. (2020). The history of nanoscience and nanotechnology: from chemical-physical applications to nanomedicine. *Molecules*, 25(1), 112.
8. Khan, I., Saeed, K., & Khan, I. (2019). Nanoparticles: Properties, applications and toxicities. *Arabian Journal of Chemistry*, 12(7), 908-931.
9. Abid, N., Khan, A. M., Shujait, S., Chaudhary, K., Ikram, M., Imran, M., Haider, J., Khan, M., Khan, Q. & Maqbool, M. (2021). Synthesis of nanomaterials using various top-down and bottom-up approaches, influencing factors, advantages, and disadvantages: A review. *Advances in Colloid and Interface Science*, 102597.
10. Khan, F. A. (2020). Synthesis of nanomaterials: methods & technology. In *Applications of Nanomaterials in Human Health* (pp. 15-21). Springer, Singapore.

11. Novoselov, K.S.; Geim, A.K.; Morozov, S.V.; Jiang, D.; Zhang, Y.; Dubonos, S.V.; Grigorieva, I.V.; Firsov, A.A. (2004). Electric Field Effect in Atomically Thin Carbon Films. *Science*, 306, 666–669.
12. Jeevanandam, J., Barhoum, A., Chan, Y. S., Dufresne, A., & Danquah, M. K. (2018). Review on nanoparticles and nanostructured materials: history, sources, toxicity and regulations. *Beilstein Journal of Nanotechnology*, 9(1), 1050-1074.
13. Arole, V. M., & Munde, S. V. (2014). Fabrication of nanomaterials by top-down and bottom-up approaches-an overview. *J. Mater. Sci*, 1, 89-93.
14. Thiyagarajan, K., Bharti, V. K., Tyagi, S., Tyagi, P. K., Ahuja, A., Kumar, K., Raj, T. & Kumar, B. (2018). Synthesis of non-toxic, biocompatible, and colloidal stable silver nanoparticle using egg-white protein as capping and reducing agents for sustainable antibacterial application. *RSC advances*, 8(41), 23213-23229.
15. Aires, A., Ocampo, S. M., Cabrera, D., de la Cueva, L., Salas, G., Teran, F. J., & Cortajarena, A. L. (2015). BSA-coated magnetic nanoparticles for improved therapeutic properties. *Journal of Materials Chemistry B*, 3(30), 6239-6247.
16. Nosrati, H., Sefidi, N., Sharafi, A., Danafar, H., & Manjili, H. K. (2018). Bovine Serum Albumin (BSA) coated iron oxide magnetic nanoparticles as biocompatible carriers for curcumin-anticancer drug. *Bioorganic Chemistry*, 76, 501-509.
17. Uthaman, S., Lee, S. J., Cherukula, K., Cho, C. S., & Park, I. K. (2015). Polysaccharide-coated magnetic nanoparticles for imaging and gene therapy. *BioMed Research International*, 2015.
18. Liu, Y., Xu, Z., Zhan, J., Li, P., & Gao, C. (2016). Superb electrically conductive graphene fibers via doping strategy. *Advanced Materials*, 28(36), 7941-7947.
19. Park, B. J., & Park, H. S. (2021). Enhanced electrical conductivity of doped graphene fiber via vacuum deposition. *Carbon Letters*, 31(4), 613-618.
20. Mohajerani, A., Burnett, L., Smith, J. V., Kurmus, H., Milas, J., Arulrajah, A., & Abdul Kadir, A. (2019). Nanoparticles in construction materials and other applications, and implications of nanoparticle use. *Materials*, 12(19), 3052.

21. Rivero, P. J., Urrutia, A., Goicoechea, J., & Arregui, F. J. (2015). Nanomaterials for functional textiles and fibers. *Nanoscale Research Letters*, 10(1), 1-22.
22. Abbasi, E., Aval, S. F., Akbarzadeh, A., Milani, M., Nasrabadi, H. T., Joo, S. W., & Pashaei-Asl, R. (2014). Dendrimers: synthesis, applications, and properties. *Nanoscale Research Letters*, 9(1), 1-10.
23. Hou, X., Zaks, T., Langer, R., & Dong, Y. (2021). Lipid nanoparticles for mRNA delivery. *Nature Reviews Materials*, 6(12), 1078-1094.
24. Yong, T., Zhang, X., Bie, N., Zhang, H., Zhang, X., Li, F., & Yang, X. (2019). Tumor exosome-based nanoparticles are efficient drug carriers for chemotherapy. *Nature Communications*, 10(1), 1-16.
25. Gregoriadis, G. (2021). Liposomes and mRNA: Two technologies together create a COVID-19 vaccine. *Medicine in Drug Discovery*, 12, 100104.
26. Tenchov, R., Bird, R., Curtze, A. E., & Zhou, Q. (2021). Lipid nanoparticles-from liposomes to mRNA vaccine delivery, a landscape of research diversity and advancement. *ACS Nano*, 15(11), 16982-17015.
27. Xu, C. Y., Inai, R., Kotaki, M., & Ramakrishna, S. (2004). Aligned biodegradable nanofibrous structure: a potential scaffold for blood vessel engineering. *Biomaterials*, 25(5), 877-886.
28. Vieira, S., Vial, S., Reis, R. L., & Oliveira, J. M. (2017). Nanoparticles for bone tissue engineering. *Biotechnology progress*, 33(3), 590-611.
29. Mehrabani, M. G., Karimian, R., Mehramouz, B., Rahimi, M., and Kafil, H. S. (2018). Preparation of biocompatible and biodegradable silk fibroin/chitin/silver nanoparticles 3D scaffolds as a bandage for antimicrobial wound dressing. *Int. J. Biol. Macromol.* 114, 961–971.
30. Zhou, L., Xu, S., Zhang, G., Cai, D., & Wu, Z. (2016). A facile approach to fabricate self-cleaning paint. *Applied Clay Science*, 132, 290-295.
31. Saad, S. R., Mahmed, N., Abdullah, M. M. A. B., & Sandu, A. V. (2016, June). Self-cleaning technology in fabric: A review. In *IOP Conference Series: Materials Science and Engineering*, 133 (1). IOP Publishing.
32. Carabineiro, S. A. (2019). Supported gold nanoparticles as catalysts for the oxidation of alcohols and alkanes. *Frontiers in Chemistry*, 7, 702.

33. Gao, C., Lyu, F., & Yin, Y. (2020). Encapsulated metal nanoparticles for catalysis. *Chemical Reviews*, 121(2), 834-881.

34. Helmlinger, J., Sengstock, C., Groß-Heitfeld, C., Mayer, C., Schildhauer, T. A., Köller, M., & Epple, M. (2016). Silver nanoparticles with different size and shape: equal cytotoxicity, but different antibacterial effects. *RSC Advances*, 6(22), 18490-18501.

35. Lundén, H., Liotta, A., Chateau, D., Lerouge, F., Chaput, F., Parola, S., Brännlund, C., Ghadyani, Z., Kildemo, M., Lindgren, M. & Lopes, C. (2015). Dispersion and self-orientation of gold nanoparticles in sol-gel hybrid silica–optical transmission properties. *Journal of Materials Chemistry C*, 3(5), 1026-1034.

36. Liu, P., Qin, R., Fu, G., & Zheng, N. (2017). Surface coordination chemistry of metal nanomaterials. *Journal of the American Chemical Society*, 139(6), 2122-2131.

37. Muthiah, M., Park, I. K., & Cho, C. S. (2013). Surface modification of iron oxide nanoparticles by biocompatible polymers for tissue imaging and targeting. *Biotechnology Advances*, 31(8), 1224-1236.

38. Li, X. M., Xu, G., Liu, Y., & He, T. (2011). Magnetic Fe3O4 nanoparticles: Synthesis and application in water treatment. *Nanoscience & Nanotechnology-Asia*, 1(1), 14-24.

39. Lakowicz, J. R. (2005). Radiative decay engineering 5: metal-enhanced fluorescence and plasmon emission. *Analytical Biochemistry*, 337(2), 171-194.

40. Bogart, L. K., Pourroy, G., Murphy, C. J., Puntes, V., Pellegrino, T., Rosenblum, D., Peer, D. & Lévy, R. (2014). Nanoparticles for imaging, sensing, and therapeutic intervention. *ACS Nano*, 8(4), 3107-3122.

41. Singh, R. K., Panigrahi, B., Mishra, S., Das, B., Jayabalan, R., Parhi, P. K., & Mandal, D. (2018). pH triggered green synthesized silver nanoparticles toward selective colorimetric detection of kanamycin and hazardous sulfide ions. *Journal of Molecular Liquids*, 269, 269-277.

42. Sengul, A. B., & Asmatulu, E. (2020). Toxicity of metal and metal oxide nanoparticles: a review. *Environmental Chemistry Letters*, 18(5), 1659-1683.

43. Petryayeva, E., & Krull, U. J. (2011). Localized surface plasmon resonance: Nanostructures, bioassays and biosensing—A review. *Analytica Chimica Acta*, 706(1), 8-24.

44. Huang, T., & Xu, X. H. N. (2010). Synthesis and characterization of tunable rainbow colored colloidal silver nanoparticles using single-nanoparticle plasmonic microscopy and spectroscopy. *Journal of Materials Chemistry*, 20(44), 9867-9876.

45. Mendis, P., de Silva, R. M., de Silva, K. N., Wijenayaka, L. A., Jayawardana, K., & Yan, M. (2016). Nanosilver rainbow: a rapid and facile method to tune different colours of nanosilver through the controlled synthesis of stable spherical silver nanoparticles. *RSC Advances*, 6(54), 48792-48799.

46. Sui, M., Kunwar, S., Pandey, P., & Lee, J. (2019). Strongly confined localized surface plasmon resonance (LSPR) bands of Pt, AgPt, AgAuPt nanoparticles. *Scientific Reports*, 9(1), 1-14.

47. Loiseau, A., Asila, V., Boitel-Aullen, G., Lam, M., Salmain, M., & Boujday, S. (2019). Silver-based plasmonic nanoparticles for and their use in biosensing. *Biosensors*, 9(2), 78.

48. Kamat, P. V. (2002). Photophysical, photochemical and photocatalytic aspects of metal nanoparticles. *The Journal of Physical Chemistry B*, 106(32), 7729-7744.

49. Toma, H. E., Zamarion, V. M., Toma, S. H., & Araki, K. (2010). The coordination chemistry at gold nanoparticles. *Journal of the Brazilian Chemical Society*, 21(7), 1158-1176.

50. Alberti, G., Zanoni, C., Magnaghi, L. R., & Biesuz, R. (2021). Gold and silver nanoparticle-based Colorimetric sensors: New trends and applications. *Chemosensors*, 9(11), 305.

51. Flores, C. Y., Diaz, C., Rubert, A., Benítez, G. A., Moreno, M. S., de Mele, M. F. L., ... & Vericat, C. (2010). Spontaneous adsorption of silver nanoparticles on Ti/TiO_2 surfaces. Antibacterial effect on Pseudomonas aeruginosa. *Journal of Colloid and Interface Science*, 350(2), 402-408.

52. Ghanizadeh Gerayeli, F., Hosseini, F., Bagheri, Z., Savardashtaki, A., Shabaninejad, Z., Amani, A. M., & Najafipour, S. (2020). Colorimetric sensor based on β-cyclodextrin-functionalized silver nanoparticles for zidovudine sensitive determination. *International Journal of Analytical Chemistry*, 2020.
53. Li, H., Li, F., Han, C., Cui, Z., Xie, G., & Zhang, A. (2010). Highly sensitive and selective tryptophan colorimetric sensor based on 4, 4-bipyridine-functionalized silver nanoparticles. *Sensors and Actuators B: Chemical*, 145(1), 194-199.
54. Shrivas, K., Sahu, J., Maji, P., & Sinha, D. (2017). Label-free selective detection of ampicillin drug in human urine samples using silver nanoparticles as a colorimetric sensing probe. *New Journal of Chemistry*, 41(14), 6685-6692.
55. Korshed, P., Li, L., Ngo, D. T., & Wang, T. (2018). Effect of storage conditions on the long-term stability of bactericidal effects for laser generated silver nanoparticles. *Nanomaterials*, 8(4), 218.
56. De Souza, C. D., Nogueira, B. R., & Rostelato, M. E. C. (2019). Review of the methodologies used in the synthesis gold nanoparticles by chemical reduction. *Journal of Alloys and Compounds*, 798, 714-740
57. Burdușel, A. C., Gherasim, O., Grumezescu, A. M., Mogoantă, L., Ficai, A., & Andronescu, E. (2018). Biomedical applications of silver nanoparticles: an up-to-date overview. *Nanomaterials*, 8(9), 681.
58. Li, W. R., Xie, X. B., Shi, Q. S., Zeng, H. Y., You-Sheng, O. Y., & Chen, Y. B. (2010). Antibacterial activity and mechanism of silver nanoparticles on Escherichia coli. *Applied Microbiology and Biotechnology*, 85(4), 1115-1122.
59. Foulkes, R., Ali Asgari, M., Curtis, A., & Hoskins, C. (2019). Silver-nanoparticle-mediated therapies in the treatment of pancreatic cancer. *ACS Applied Nano Materials*, 2(4), 1758-1772.
60. Behzadifar, S., Hosseini, M., Mohammadnejad, J., & Asiabanha, M. (2021). A new colorimetric assay for sensitive detection of glucose-6-phosphate dehydrogenase deficiency based on silver nanoparticles. *Nanotechnology*, 33(5), 055502.

61. Ahmed, F., Kabir, H., & Xiong, H. (2020). Dual colorimetric sensor for Hg^{2+}/Pb^{2+} and an efficient catalyst based on silver nanoparticles mediating by the root extract of bistorta amplexicaulis. *Frontiers in Chemistry*, 945.
62. Roto, R., Mellisani, B., Kuncaka, A., Mudasir, M., & Suratman, A. (2019). Colorimetric sensing of Pb^{2+} ion by using ag nanoparticles in the presence of dithizone. *Chemosensors*, 7(3), 28.
63. Kodir, A., Imawan, C., Permana, I. S., & Handayani, W. (2016, August). Pesticide colorimetric sensor based on silver nanoparticles modified by L-cysteine. In *2016 International Seminar on Sensors, Instrumentation, Measurement and Metrology (ISSIMM)* (pp. 43-47). IEEE.
64. Eswaran, S. G., Ashkar, M. A., Mamat, M. H., Sahila, S., Mahalingam, V., Koppisetti, H. V. S. R. M., & Vasimalai, N. (2021). Preparation of a portable calorimetry kit and one-step spectrophotometric nanomolar level detection of L-Histidine in serum and urine samples using sebacic acid capped silver nanoparticles. *Journal of Science: Advanced Materials and Devices*, 6(1), 100-107.
65. Thompson, D. G., Enright, A., Faulds, K., Smith, W. E., & Graham, D. (2008). Ultrasensitive DNA detection using oligonucleotide− silver nanoparticle conjugates. *Analytical Chemistry*, 80(8), 2805-2810.
66. Ma, X., & Miao, P. (2019). Silver nanoparticle@ DNA tetrahedron-based colorimetric detection of HIV-related DNA with cascade strand displacement amplification. *Journal of Materials Chemistry B*, 7(16), 2608-2612.
67. Jain PK, Huang X, El-Sayed IH, El-Sayed MA. (2008). Noble metals on the nanoscale: optical and photothermal properties and some applications in imaging, sensing, biology and medicine. *Acc. Chem. Res.* 41(12), 1578–1586.
68. Kelly KL, Coronado E, Zhao LL, Schatz GC. The optical properties of metal nanoparticles: the influence of size, shape and dielectric environment. *J. Phys. Chem. B* 107(3), 668–677 (2003).
69. Rawat, K. A., Singhal, R. K., & Kailasa, S. K. (2017). One-pot synthesis of silver nanoparticles using folic acid as a reagent for colorimetric and fluorimetric

detections of 6-mercaptopurine at nanomolar concentration. *Sensors and Actuators B: Chemical*, 249, 30-38.

70. Food and Drug Administration Compliance Program Manual (Program 7356.002F), dated 13 February, 2006, Chapter 56, Drug Quality Assurance at 4.
71. Meadows, D. (1996). Recent developments with biosensing technology and applications in the pharmaceutical industry. *Advanced Drug Delivery Reviews*, 21(3), 179-189.
72. Ghodake, G., Shinde, S., Saratale, R. G., Kadam, A., Saratale, G. D., Syed, A., Marraiki, N., Elgorban, A. M. & Kim, D. Y. (2020). Silver nanoparticle probe for colorimetric detection of aminoglycoside antibiotics: picomolar- level sensitivity toward streptomycin in water, serum, and milk samples. *Journal of the Science of Food and Agriculture*, 100(2), 874-884.
73. Mahoney, E., Kun, J., Smieja, M., & Fang, Q. (2019). Point-of-care urinalysis with emerging sensing and imaging technologies. *Journal of the Electrochemical Society*, 167(3), 037518.
74. Moraes, L. D. D. M., Oliveira, A. F. D., Teixeira, A. V. D. C., & Lopes, R. P. (2020). Method development and validation for the fluoroquinolones determination by stabilized silver nanoparticles. *Química Nova*, 43, 271-278.
75. Piconi, S., Parisotto, S., Rizzardini, G., Passerini, S., Terzi, R., Argenteri, B., Meraviglia, P., Capetti, A., Biasin, M., Trabattoni, D. & Clerici M. (2011). Hydroxychloroquine drastically reduces immune activation in HIV-infected, antiretroviral therapy–treated immunologic nonresponders. *Blood, The Journal of the American Society of Hematology*, 118(12), 3263-3272.
76. Ghose, M., Patel, M., & Nugent, K. (2020). Hydroxychloroquine: A review of its effects on viral replication based on current literature. *The Southwest Respiratory and Critical Care Chronicles*, 8(36), 47-54.
77. Tett, S., McLachlan, A., Day, R., & Cutler, D. (1993). Insights from pharmacokinetic and pharmacodynamic studies of hydroxychloroquine. *Agents and Actions. Supplements*, 44, 145-190.

78. Baildya, N., Ghosh, N. N., & Chattopadhyay, A. P. (2020). Inhibitory activity of hydroxychloroquine on COVID-19 main protease: An insight from MD-simulation studies. *Journal of Molecular Structure*, 1219, 128595.
79. Shippey, E. A., Wagler, V. D., Collamer, A. N. (2018). Hydroxychloroquine: An old drug with new relevance. *Cleve Clin J Med*., 85(6):459-467.
80. Ben-Zvi, I., Kivity, S., Langevitz, P., & Shoenfeld, Y. (2012). Hydroxychloroquine: from malaria to autoimmunity. *Clinical Reviews in Allergy & Immunology*, 42(2), 145-153.
81. Liu, J., Cao, R., Xu, M., Wang, X., Zhang, H., Hu, H., Yufeng, L., Hu, Z., Zhong, W. & Wang, M. (2020). Hydroxychloroquine, a less toxic derivative of chloroquine, is effective in inhibiting SARS-CoV-2 infection in vitro. *Cell Discovery*, 6(1), 1-4.
82. Furst, D. E. (1996). Pharmacokinetics of hydroxychloroquine and chloroquine during treatment of rheumatic diseases. *Lupus*, 5(1_suppl), 11-15.
83. Solitro, A. R., & MacKeigan, J. P. (2016). Leaving the lysosome behind: novel developments in autophagy inhibition. *Future Medicinal Chemistry*, 8(1), 73-86.
84. Nagaraja, B. S., Ramesh, K. N., Dhar, D., Mondal, M. S., Dey, T., Saha, S. & Singh, V. (2020). HyPE study: hydroxychloroquine prophylaxis-related adverse events' analysis among healthcare workers during COVID-19 pandemic: a rising public health concern. *Journal of Public Health*, 42(3), 493-503.
85. Browning, D. J. (2014). Pharmacology of chloroquine and hydroxychloroquine. In hydroxychloroquine and chloroquine retinopathy (pp. 35-63). Springer, New York, NY.
86. Chatre, C., Roubille, F., Vernhet, H., Jorgensen, C., & Pers, Y. M. (2018). Cardiac complications attributed to chloroquine and hydroxychloroquine: a systematic review of the literature. *Drug Safety*, 41(10), 919-931.
87. FDA/CDER. Plaquenil® Hydroxychloroquine Sulfate Tablets, Usp Description. FDA, 2017. From

https://www.accessdata.fda.gov/drugsatfda_docs/label/2017/009768s037s045s047lbl.pdf, retrieved 23.03.2022.

88. Bilgin, Z. D., Evcil, I., Yazgi, D., Binay, G., Okuyucu Genc, C., Gulsen, B. & Caglar Andac, S. (2021). Liquid chromatographic methods for COVID-19 drugs, hydrhrioxychloroquine and chloroquine. *Journal of Chromatographic Science*, 59(8), 748-757.
89. Della Porta, A., Bornstein, K., Coye, A., Montrief, T., Long, B., & Parris, M. A. (2020). Acute chloroquine and hydroxychloroquine toxicity: A review for emergency clinicians. *The American Journal of Emergency Medicine*, 38(10), 2209-2217.
90. Ambrus, C., Bakos, É., Sarkadi, B., Özvegy-Laczka, C., & Telbisz, Á. (2021). Interactions of anti-COVID-19 drug candidates with hepatic transporters may cause liver toxicity and affect pharmacokinetics. *Scientific Reports*, 11(1), 1-10.
91. Karatza, E., Ismailos, G., Marangos, M., & Karalis, V. (2021). Optimization of hydroxychloroquine dosing scheme based on COVID-19 patients' characteristics: a review of the literature and simulations. *Xenobiotica*, 51(2), 127-138.
92. Zhang, T. Y., & Zhong, B. (2020). Meeting the potential emergency global drug supply challenge of hydroxychloroquine for COVID-19. *Medicine in Drug Discovery*, 5, 100036.
93. Pagliaro, M., & Meneguzzo, F. (2020). Hydroxychloroquine for the treatment of coronavirus disease 2019: Evidence, possible mode of action and industrial supply. *Medicine Research*, 4(3), 200014.
94. Mukherjee, R. (2020, April 8). Zydus Cadila boosts HCQ production 10X. *The Times of India.*
95. Katiyar, P. (2020, April 13). Hydroxychloroquine production scaled up: Zydus Cadila. *The Times of India.*
96. Soomro, R. A. (2020). Development of biosensors for drug detection applications. *Nanobiosensors: From Design to Applications*, 203-222.

97. Sumpter, J. P. (2010). Pharmaceuticals in the environment: Moving from a problem to a solution. In *Green and Sustainable Pharmacy* (pp. 11-22). Springer, Berlin, Heidelberg.

98. 4 European Environmental Bureau. (n.d.). The environmental and health impacts caused by emissions of APIs to the environment. http://eeb.org/publications/31/chemicals/89561/briefing-on-the-environmental-and-health-impacts-of-active-pharmaceuticals-ingredients.pdf

99. Wilkinson, J. L., Boxall, A. B., Kolpin, D. W., Leung, K. M., Lai, R. W., Galbán-Malagón, C., et al. (2022). Pharmaceutical pollution of the world's rivers. *Proceedings of the National Academy of Sciences*, 119(8), e2113947119.

100. Bloland, P. B., & World Health Organization. (2001). Drug resistance in malaria (No. WHO/CDS/CSR/DRS/2001.4). World Health Organization.

101. Quashie, N. B., & Duah-Quashie, N. O. (2021). Treatment of COVID-19 with chloroquine: Implication for malaria chemotherapy using ACTs in disease endemic countries. *Journal of Tropical Pediatrics*, 67(1), fmaa089.

102. Lee, S. W., Lee, M., Lee, D. D., Kim, C., Kim, Y. J., Kim, J. Y., et al. (2009). Biological resistance of hydroxychloroquine for Plasmodium vivax malaria in the Republic of Korea. *Am J Trop Med Hyg*. 2009 Oct;81(4):600-4

103. Morris, R. G. (1985). Estimation of plasma hydroxychloroquine by high-performance liquid chromatography with ultraviolet detection. *Journal of Chromatography B: Biomedical Sciences and Applications*, 338, 422-427

104. Bodur, S., Erarpat, S., Günkara, Ö. T., & Bakırdere, S. (2021). Accurate and sensitive determination of hydroxychloroquine sulfate used on COVID-19 patients in human urine, serum and saliva samples by GC-MS. *Journal of Pharmaceutical Analysis*, 11(3), 278-283.

105. Williams, S. B., Patchen, L. C., & Churchill, F. C. (1988). Analysis of blood and urine samples for hydroxychloroquine and three major metabolites by high-performance liquid chromatography with fluorescence detection. *Journal of Chromatography B: Biomedical Sciences and Applications*, 433, 197-206.

106. Tett, S. E., Cutler, D. J., & Brown, K. F. (1985). High-performance liquid chromatographic assay for hydroxychloroquine and metabolites in blood and

plasma, using a stationary phase of poly (styrene divinylbenzene) and a mobile phase at pH 11, with fluorimetric detection. *Journal of Chromatography B: Biomedical Sciences and Applications*, 344, 241-248.

107. Xiong, X., Wang, K., Tang, T., Fang, J., & Chen, Y. (2021). Development of a chiral HPLC method for the separation and quantification of hydroxychloroquine enantiomers. *Scientific Reports*, 11(1), 1-7.

108. Rahimi, F., Chatzimichail, S., Saifuddin, A., Surman, A. J., Taylor-Robinson, S. D., & Salehi-Reyhani, A. (2020). A review of portable high-performance liquid chromatography: The future of the Field?. *Chromatographia*, 83(10), 1165-1195.

109. Delhomme, O., & Millet, M. (2008). Comparison of two analytical methods for the determination of azaarenes in atmospheric particulate matter. *Polycyclic Aromatic Compounds*, 28(4-5), 518-532.

110. Farthing, C. A., Farthing, D. E., Koka, S., Larus, T., Fakhry, I., Xi, L., Kukreja, R. C., Sica, D. & Gehr, T. W. (2010). A simple and sensitive HPLC fluorescence method for determination of tadalafil in mouse plasma. *Journal of Chromatography* B, 878(28), 2891-2895.

111. Arguelho, M. L. P., Andrade, J. F., & Stradiotto, N. R. (2003). Electrochemical study of hydroxychloroquine and its determination in plaquenil by differential pulse voltammetry. *Journal of Pharmaceutical and Biomedical Analysis*, 32(2), 269-275.

112. Mashhadizadeh, M. H., & Akbarian, M. (2009). Voltammetric determination of some anti-malarial drugs using a carbon paste electrode modified with $Cu(OH)_2$ nano-wire. *Talanta*, 78(4-5), 1440-1445.

113. Deroco, P. B., Vicentini, F. C., Oliveira, G. G., Rocha-Filho, R. C., & Fatibello-Filho, O. (2014). Square-wave voltammetric determination of hydroxychloroquine in pharmaceutical and synthetic urine samples using a cathodically pretreated boron-doped diamond electrode. *Journal of Electroanalytical Chemistry*, 719, 19-23.

114. Khoobi, A., Ghoreishi, S. M., Behpour, M., Shaterian, M., & Salavati-Niasari, M. (2014). Design and evaluation of a highly sensitive nanostructure-based

surface modification of glassy carbon electrode for electrochemical studies of hydroxychloroquine in the presence of acetaminophen. *Colloids and Surfaces B: Biointerfaces*, 123, 648-656.

115. Khalil MM, Issa YM, El Sayed GA (2015). Development of a new coated graphite electrode for hydroxychloroquine sulfate determination in pharmaceutical preparations and human urine. *Int. J. Adv. Res.* 3, 592–603

116. Pushpanjali, P. A., Manjunatha, J. G., Hareesha, N., Girish, T., Al-Kahtani, A. A., Tighezza, A. M., & Ataollahi, N. (2022). Electrocatalytic determination of hydroxychloroquine using Sodium dodecyl sulphate modified carbon nanotube paste electrode. *Topics in Catalysis*, 1-9.

117. Khoobi, A., Ghoreishi, S. M., & Behpour, M. (2014). Sensitive and selective determination of hydroxychloroquine in the presence of uric acid using a new nanostructure self-assembled monolayer modified electrode: optimization by multivariate data analysis. *Analyst*, 139(16), 4064-4072.

118. Paramelle, D., Sadovoy, A., Gorelik, S., Free, P., Hobley, J., & Fernig, D. G. (2014). A rapid method to estimate the concentration of citrate capped silver nanoparticles from UV-visible light spectra. *Analyst*, 139(19), 4855-4861.

119. Mao, Q., Kong, X., Shuang, E., Wang, J., & Chen, X. (2020). Preparation of silver nanoparticles with ionic liquid-modified carbon dots: from mechanism to the application in H_2O_2 sensing. *Journal of Materials Science*, 55(36), 16928-16939

120. Walekar, L. S., Hu, P., Liao, F., Guo, X., & Long, M. (2018). Turn-on fluorometric and colorimetric probe for hydrogen peroxide based on the in-situ formation of silver ions from a composite made from N-doped carbon quantum dots and silver nanoparticles. *Microchimica Acta*, 185(1), 1-9.

121. Sangaonkar, G. M., Desai, M. P., Dongale, T. D., & Pawar, K. D. (2020). Selective interaction between phytomediated anionic silver nanoparticles and mercury leading to amalgam formation enables highly sensitive, colorimetric and memristor-based detection of mercury. *Scientific Reports*, 10(1), 1-12.

122. Usta, H. M., Forough, M., & Çetinkol, Ö. P. (2019). A DNA-free colorimetric probe based on citrate-capped silver nanoparticles for sensitive and rapid detection of coralyne. *Sensors and Actuators B: Chemical*, 298, 126823.

123. Niesser, M., Koletzko, B., & Peissner, W. (2012). Determination of creatinine in human urine with flow injection tandem mass spectrometry. *Annals of Nutrition and Metabolism*, 61(4), 314-321.

124. Beretov, J., Wasinger, V. C., Schwartz, P., Graham, P. H., & Li, Y. (2014). A standardized and reproducible urine preparation protocol for cancer biomarkers discovery. *Biomarkers in Cancer*, 6, BIC-S17991.

125. Taylor, T. P., Janech, M. G., Slate, E. H., Lewis, E. C., Arthur, J. M., & Oates, J. C. (2012). Overcoming the effects of matrix interference in the measurement of urine protein analytes. *Biomarker Insights*, 7, BMI-S8703.

126. Hewavitharana, A. K., Tan, S. K., & Shaw, P. N. (2014). Strategies for the detection and elimination of matrix effects in quantitative LC-MS analysis. *LC-GC North America*, 32(1), 54-64.

127. Gutierrez, L., Schmid, A., Zaouri, N., Garces, D., & Croue, J. P. (2020). Colloidal stability of capped silver nanoparticles in natural organic matter-containing electrolyte solutions. *NanoImpact*, 19, 100242.

128. El Badawy, A. M., Scheckel, K. G., Suidan, M., & Tolaymat, T. (2012). The impact of stabilization mechanism on the aggregation kinetics of silver nanoparticles. *Science of the Total Environment*, 429, 325-331.

129. Bélteky, P., Rónavári, A., Igaz, N., Szerencsés, B., Tóth, I. Y., Pfeiffer, I., Kirisci, M. & Kónya, Z. (2019). Silver nanoparticles: aggregation behavior in biorelevant conditions and its impact on biological activity. *International Journal of Nanomedicine*, 14, 667.

130. Huynh, K. A., & Chen, K. L. (2011). Aggregation kinetics of citrate and polyvinylpyrrolidone coated silver nanoparticles in monovalent and divalent electrolyte solutions. *Environmental Science & Technology*, 45(13), 5564-5571.

131. Baalousha, M., Nur, Y., Römer, I., Tejamaya, M., & Lead, J. R. (2013). Effect of monovalent and divalent cations, anions and fulvic acid on aggregation of

citrate-coated silver nanoparticles. *Science of the Total Environment*, 454, 119-131.

132. Li, X., Lenhart, J. J., & Walker, H. W. (2012). Aggregation kinetics and dissolution of coated silver nanoparticles. *Langmuir*, 28(2), 1095-1104.

133. Velgosova, O., Čižmárová, E., Málek, J., & Kavuličova, J. (2017). Effect of storage conditions on long-term stability of Ag nanoparticles formed via green synthesis. *International Journal of Minerals, Metallurgy, and Materials*, 24(10), 1177-1182.

134. Izak-Nau, E., Huk, A., Reidy, B., Uggerud, H., Vadset, M., Eiden, S., et al. (2015). Impact of storage conditions and storage time on silver nanoparticles' physicochemical properties and implications for their biological effects. *RSC Advances*, 5(102), 84172-84185.

135. Schroeder, R. L., & Gerber, J. P. (2014). Chloroquine and hydroxychloroquine binding to melanin: some possible consequences for pathologies. *Toxicology Reports*, 1, 963-968.

136. Warhurst, D. C., Steele, J. C., Adagu, I. S., Craig, J. C., & Cullander, C. (2003). Hydroxychloroquine is much less active than chloroquine against chloroquine-resistant Plasmodium falciparum, in agreement with its physicochemical properties. *Journal of Antimicrobial Chemotherapy*, 52(2), 188-193.

137. Garcia- Cremades, M., Solans, B. P., Hughes, E., Ernest, J. P., Wallender, E., Aweeka, F., et al. (2020). Optimizing hydroxychloroquine dosing for patients with COVID- 19: an integrative modeling approach for effective drug repurposing. *Clinical Pharmacology & Therapeutics*, 108(2), 253-263.

138. El Badawy, A. M.; Luxton, T. P.; Silva, R. G.; Scheckel, K. G.; Suidan, M. T.; Tolaymat, T. M. (2010). Impact of environmental conditions (pH, ionic strength, and electrolyte type) on the surface charge and aggregation of silver nanoparticles suspensions. *Environ. Sci. Technol.*, 44 (4), 1260−1266.

139. Yin, Y.; Li, Z. Y.; Zhong, Z.; Gates, B.; Xia, Y.; Venkateswaran, S. Synthesis and characterization of stable aqueous dispersions of silver nanoparticles through the Tollens process. *J. Mater. Chem*. 2002, 12, 522−527.

140. Levard, C., Mitra, S., Yang, T., Jew, A. D., Badireddy, A. R., Lowry, G. V., & Brown Jr, G. E. (2013). Effect of chloride on the dissolution rate of silver nanoparticles and toxicity to E. coli. *Environmental Science & Technology, 47*(11), 5738-5745.

141. Treasa, M. S., & Premakumari, J. (2018). Characterisation and solubility studies of quinine sulphate and hydroxychloroquine sulphate inclusion complexes with α–cyclodextrin. *IOSR J. Appl. Chem.(IOSR-JAC)*, 11, 24-34.

142. Zou, X., Ying, E., & Dong, S. (2006). Seed-mediated synthesis of branched gold nanoparticles with the assistance of citrate and their surface-enhanced Raman scattering properties. *Nanotechnology*, 17(18), 4758.

143. Zhu, T., Vasilev K., Kreiter M., Mittler S. & Knoll W. (2003). Surface modification of citrate-reduced colloidal gold nanoparticles with 2-mercaptosuccinic acid, *Langmuir*, 19 , 9518 —9525

144. M. Dakanali, E. T. Kefalas, C. P. Raptopoulou, A. Terzis, T. Mavromoustakos and A. Salifoglou (2003). Synthesis and spectroscopic and structural studies of a new cadmium(II)–citrate aqueous complex. Potential relevance to cadmium(II)–citrate speciation and links to cadmium toxicity, *Inorg. Chem*., 42, 2531-2537

145. Alam, S., Kamal, T. B., Sarker, M. M. R., Zhou, J. R., Rahman, S. A., & Mohamed, I. N. (2021). Therapeutic effectiveness and safety of repurposing drugs for the treatment of COVID-19: position standing in 2021. *Frontiers in Pharmacology*, 12.

146. Morad, R., Akbari, M., Rezaee, P., Koochaki, A., Maaza, M., & Jamshidi, Z. (2021). First principle simulation of coated hydroxychloroquine on Ag, Au and Pt nanoparticles. *Scientific Reports*, 11(1), 1-9.

147. Martínez, A. (2020). Cloroquine and hydroxychloroquine: the Yin-yang of these drugs from a theoretical study. *Journal of the Mexican Chemical Society*, 64(3), 230-237.

148. Sykes, B. D. (2007). Urine stability for metabolomic studies: effects of preparation and storage. *Metabolomics*, 3(1), 19-27.

APPENDIX

A. Stability of Cit-AgNPs with Temperature and Time

AgNPs' stability alone is also thought to be an important factor in obtaining accurate and reliable results in our Cit-AgNPs+NaCl+HCQ platform. Therefore, the stability of AgNPs with time was also assessed as a control. Previous studies reported that AgNPs can be stored in argon-saturated ultrapure water to avoid dissolution and they should be kept in dark to prevent photochemical aging. It was reported that, those storage conditions maintained colloidal stability for at least 6 months [55]. In the case of Cit-AgNPs, repulsion between negatively charged citrate ions stabilizes the nanoparticles. However, over time the interactions of these capping agents with other constituents in solution (e.g. H_2O, electrolytes) change the physicochemical properties of AgNPs' surface and result in aggregation [127]. Several reports revealed the importance of stroge conditions (time and temperature) on AgNPs agglomeration. The AgNPs are reported to agglomerate at room temperature during prolonged times. And the temperature is reported to increase the agglomeration behavior of AgNPs, possibly due to the increased collisions between the particles [133, 134].

In order to reveal the stability of Cit-AgNPs, synthesized Cit-AgNPs were diluted with H_2O and were stored either at room temperature (RT) or 4 ^oC. The lids of containers were sealed with parafilm to minimize contaminations from ventilation or chemical splits. The UV-Vis spectra of Cit-AgNPs, stored under different conditions, were taken at different times (Figures A1 and A2).

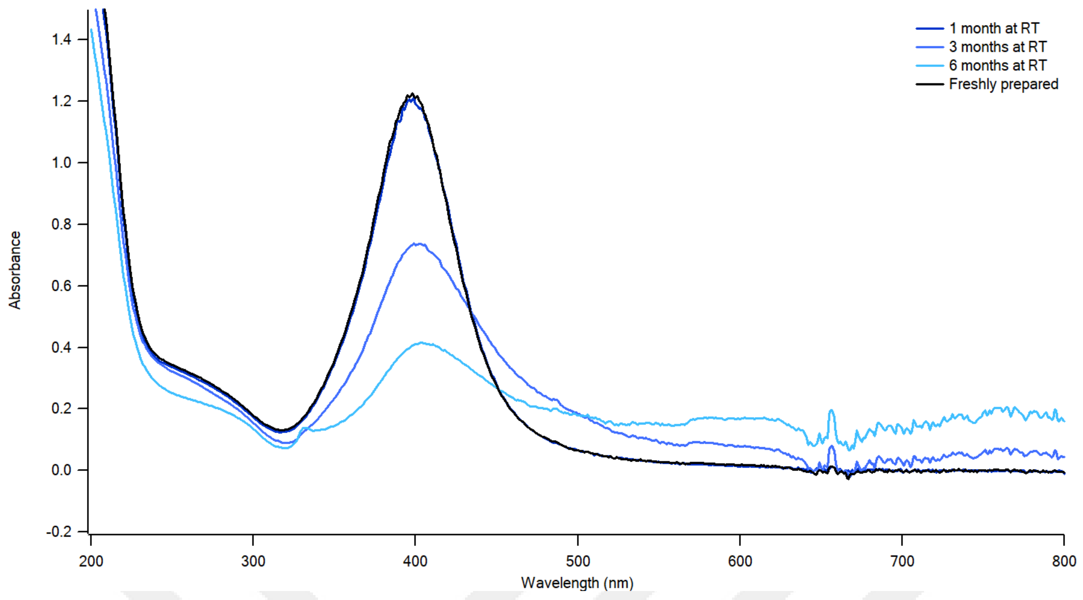

Figure 20: UV-Vis spectra of Cit-AgNPs stored at room temperature for different time periods.

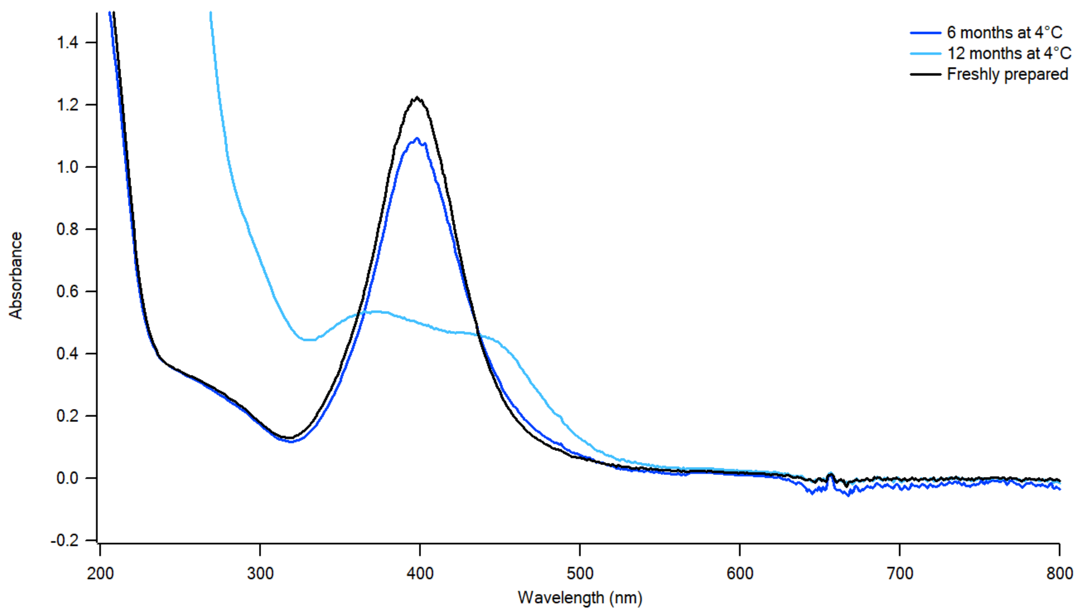

Figure 21: UV-Vis spectra of Cit-AgNPs stored at 4 ^{o}C for different time periods.

As displayed in Figure A1, freshly prepared Cit-AgNPs (black spectrum) at room temperature were stable at least 1 month after the synthesis (navy spectrum) while the LSPR signal significantly decreased and broadened after 3 months (blue spectrum). The colors of 1 month, 3 months and 6 months old samples were shiny yellow, yellow-green and olive green respectively (data not shown) which indicated the formation of larger Cit-AgNPs in the solutions for the last two samples [44, 45]. The samples stored in the refrigerator exhibited a slightly reduced LSPR signal after 6 months (Figure A2, blue spectrum) compared to reduction of the LSPR signal of the sample stored at RT (Figure A1, light blue spectrum). Therefore, Cit-AgNPs were stored at 4 ^{o}C in the dark in sealed containers to increase their durability throughout the experiments. Moreover, to ensure their stable structure, UV-Vis spectra of Cit-AgNPs were taken before all experiments and those spectra were compared to the spectrum taken when they were freshly prepared.